ANALYSIS OF A CALIBRATION METHOD FOR AIRBORNE RECEIVE ONLY PHASED ARRAY ANTENNAS WITH SELF-ALIGNMENT

A THESIS SUBMITTED TO
THE GRADUATE SCHOOL OF NATURAL AND APPLIED SCIENCES
OF
MIDDLE EAST TECHNICAL UNIVERSITY

BY

FURKAN BAHADIR ELİK

IN PARTIAL FULFILLMENT OF THE REQUIREMENTS
FOR
THE DEGREE OF MASTER OF SCIENCE
IN
ELECTRICAL AND ELECTRONIC ENGINEERING

SEPTEMBER 2022

Approval of the thesis:

ANALYSIS OF A CALIBRATION METHOD FOR AIRBORNE RECEIVE ONLY PHASED ARRAY ANTENNAS WITH SELF-ALIGNMENT

submitted by **FURKAN BAHADIR ELİK** in partial fulfillment of the requirements for the degree of **Master of Science** i**n Electrical and Electronic Engineering, Middle East Technical University** by,

Prof. Dr. Halil Kalıpçılar
Dean, Graduate School of **Natural and Applied Sciences** _____

Prof. Dr. İlkay Ulusoy
Head of the Department, **Electrical and Electronics Eng.** _____

Prof. Dr. Şimşek Demir
Supervisor, **Electrical and Electronics Engineering, METU** _____

Examining Committee Members:

Prof. Dr. Gülbin Dural
Electrical and Electronics Engineering, METU _____

Prof. Dr. Şimşek Demir
Electrical and Electronics Engineering, METU _____

Prof. Dr. Gönül Turhan Sayan
Electrical and Electronics Engineering, METU _____

Prof. Dr. Özlem Aydın Çivi
Electrical and Electronics Engineering., METU _____

Prof. Dr. Özlem Özgün
Electrical and Electronics Engineering Hacettepe University _____

Date: 15.09.2022

I hereby declare that all information in this document has been obtained and presented in accordance with academic rules and ethical conduct. I also declare that, as required by these rules and conduct, I have fully cited and referenced all material and results that are not original to this work.

Name Last name : Furkan Bahadır Elik

Signature :

ABSTRACT

ANALYSIS OF A CALIBRATION METHOD FOR AIRBORNE RECEIVE-ONLY PHASED ARRAY ANTENNAS WITH SELF-ALIGNMENT

Elik, Furkan Bahadır
Master of Science, Electrical and Electronic Engineering
Supervisor : Prof. Dr. Şimşek Demir

September 2022, 71 pages

The calibration of the phased array antennas plays crucial role to ensure the performance of the beam steering capability. Most of the guided missiles utilize phased arrays, thus, the calibration routines should be optimized. Since guided missiles are spatially limited, calibration hardware should not introduce new geometry to the antenna. This limits possible calibration methods of the antennas on the missiles. This study develops a calibration method for semi-active guided missiles and analyzes this method in terms of performance and feasibility in the simulation environment. In order to find the most suitable method, the mutual coupling and the peripheral fixed probes methods are discussed thoroughly and combined to develop a hybrid method to achieve self-calibration capability without any additional geometry to the antenna. First, an 8×4 phased array antenna is designed at 10 GHz center frequency with 200MHz bandwidth as the simulation environment. Later, reference antennas are assigned concerning the proposed method. For the error modeling, an RMS error with peak phase error of 40 degrees is introduced to each phase shifter in the array. To align phases, the remapping of the phase states is implemented as the algorithm.

Keywords: Phased Array Antenna, Antenna Calibration, Self-alignment, Mutual Coupling, Peripheral Fixed Probes

ÖZ

HAVA PLATFORMLARI İÇİN ALICI FAZ DİZİLİ ANTENLERDE KENDİNİ AYARLAYAN KALİBRASYON YÖNTEMİNİN İNCELENMESİ

Elik, Furkan Bahadır
Yüksek Lisans, Elektrik ve Elektronik Mühendisliği
Tez Yöneticisi: Prof. Dr. Şimşek Demir

Eylül 2022, 71 sayfa

Faz dizili antenlerde anten kalibrasyonu, hüzme yönlendirme yeteneğinin performansı izin kritik rol oynamaktadır. Çoğu güdümlü füzelerde faz dizili anten kullanıldığından, kalibrasyon rutinleri füzeler için optimize edilmelidir. Fakat, füzeler hacim olarak limitli olduğundan, kullanılacak kalibrasyon yöntemi antene fazladan bir geometri katmamalıdır. Bu durum, füzelerde uygulanabilecek kalibrasyon yöntemini kısıtlar. Bu çalışmada, yarı-aktif güdümlü füzelerde uygulanmak üzere bir kalibrasyon yöntemi geliştirip, bu yöntemin benzetim ortamında uygulanabilirliği irdelenmiştir. En uygun method bulmak için müşterek bağlaşım ve çevresel sabit yoklayıcı yöntemleri detaylı bir şekilde incelenip birleştirilerek, kendini ayarlayabilen ve ek anten geometrisi sunmayan hibrit bir method geliştirilmiştir. İlk olarak, 8×4 boyutunda, 10 GHz merkez frekansında 200 MHz bant genişliğine sahip bir faz dizili anten oluşturulmuştur. Sonrasında, referans antenler, hibrit methoda göre seçilmiştir. Hata modellemesi için, en yüksek 40 derece faz hatalı kök-kare-ortalamalı hata anten dizisindeki her faz kaydırıcı için eklenmiştir. Hatalı fazların tekrar ayarlanması için, algoritma olarak, faz kaydırıcıların faz durumları yeniden atanarak istenilen faz kaydırma değerlerine ulaşılmıştır.

Anahtar Kelimeler: Faz Dizili Antenler, Anten Kalibrasyonu, Kendini Ayarlayan Antenler, Müşterek Bağlaşım, Çevresel Sabit Yoklayıcı

To those who dedicate themselves to humanity and the nature

ACKNOWLEDGMENTS

First, I would like to express my deepest gratitude to my supervisor Prof. Dr. Şimşek Demir for his valuable technical support, guidance, and encouragements throughout my master's program. Since my bachelor's, his perspective for engineering led me to pursue my carrier as an RF engineer.

I would like to thank my examining committee, Prof. Dr. Gülbin Dural, Prof. Dr. Gönül Turhan Sayan, Prof. Dr. Özlem Aydın Çivi and Prof Dr. Özlem Özgün for their valuable time, inspiring comments, and contributions during the thesis examination.

Also, I must express my deepest gratitude to my family for their endless support throughout my life. My mother, Hatice Elik has been my greatest mentor, whom I can talk to and discuss anything. Also, I am thankful to my father, Mustafa Elik who enabled me to become curios about science and nature. They taught me how to overcome any obstacle I encounter, and they made me who I am today. I could not be more grateful for this. I also thank my little brother, Buğra Mert Elik, for always being by my side as my closest friend. Without them, I would not be able to achieve what I have today. Finally, my deepest gratitude is for my grandmother, Sabiha Yıldız, who took care of us as children and raised us; may she rest in peace.

I would like to thank and express my love to Lale Tunçbilek, who was very supportive, encouraging and patient throughout this thesis journey. I feel extremely lucky to have her in my life. Completing our theses side by side was a delightful activity and marks an indelible memory in my mind. Also, I am thankful to my cat, Isaac, for his endless love, distraction, and amusement.

I am thankful to all of my friends for their support and understanding for my absence. My special thanks to Mustafa Işık, Zafer Türk, Barkın Durmuş and Levent Oktay for their valuable friendship. I am grateful to have you all in my life.

In addition, sincere thanks to Roketsan Missiles Inc. for supporting my studies and providing such a progressive environment. Also, I would like to thank all of my colleagues for their technical support during this thesis. Special thanks to Caner Önder and Türker Dolapçı for their valuable advice and supports on CST and overall thesis study. Also, I would like to thank to Mutlu Koldaş for helping me out with the MATLAB and CST scripting.

I am thankful to TÜBİTAK for supporting my graduate studies with 2210A National Scholarship Program.

Finally, I feel my deepest gratitude to Atatürk, for founding this country and enabling me to be grow and become a good engineer.

TABLE OF CONTENTS

LIST OF TABLES

TABLES

LIST OF FIGURES

FIGURES

LIST OF ABBREVIATIONS

ABBREVIATIONS	
ADC	Analog to Digital Converter
AUT	Antenna Under Test
API	Application Programming Interface
dB	Decibel
DUT	Device Under Test
DSP	Digital Signal Processing
ESA	Electronically Steered Antenna
GaAs	Gallium Arsenide
GaN	Gallium Nitride
GNSS	Global Navigation Satellite System
HEMT	High Electron Mobility Transistor
IC	Integrated Circuit
IF	Intermediate Frequency
INS	Inertial Navigation System
IR	Infrared Radiation
I-Q	In-phase and Quadrature
Ka	Kurtz
Ku	Kurtz Under
LNA	Low Noise Amplifier
LUT	Look Up Table
MATLAB	Matrix Laboratory
MEMS	Micro Electromechanical Systems
MMIC	Monolithic Microwave Integrated Circuit
PA	Power Amplifier
pHEMT	Pseudomorphic High Electron Mobility Transistor
RF	Radio Frequency
RMS	Root Mean Square
Rx	Receiver

SLL	Side Lobe Level
SNR	Signal to Noise Ratio
T/R	Transmit/Receive
Tx	Transmitter
VGA	Variable Gain Amplifier
VNA	Vector Network Analyzer

CHAPTER 1

INTRODUCTION

With the developing technology and the current trends towards radar systems in aerial vehicles and increasing speed of communications techniques, there is an increasing interest for higher accuracy, higher speeds with higher complexity of the systems. Considering cutting-edge aerial vehicles, that is, supersonic planes, ballistic and cruise missiles, communications satellites, and space rockets, there is a non-deniable requirement for increased durability, automated operation, and higher efficiency for electrical systems. These electrical subsystems may include radars, navigation systems, and high-speed data links.

Considering radars, it is desired to have the ability to detect and track the target with less uncertainty, fewer and more agile hardware, hence, more responsive and reliable systems. Such capabilities for radars can be achieved through both hardware and software improvements. From RF engineering point of view, such hardware improvements may include using components with lower noise figures, using ADCs (Analog to Digital Converter) with higher resolution and higher sampling rate, or using better antennas. From this list, if we focus on the antennas, it can be seen that the antenna design approach and technique play a significant role in the different playgrounds that the techniques offer. In other words, while most hardware improvements depend on better numbers, higher SNR (Signal to Noise Ratio) or lower levels of spurs, the antenna of the system can be improved not only by the numbers it can offer, higher gain or lower SLL (Side Lobe Level), but by the design technique it depends on having a significant effect.

Antenna design typologies for Radars have been developed significantly over the years. To locate the target of interest, the antenna beam must align itself with the RF

signature of the target. Only then, if the receiver block is sensitive enough to decode received RF signals, can the target be appropriately acquired. For this objective, firstly, mechanically steered antennas have been introduced to the market. This topology includes a fixed antenna (usually an array antenna or dish antenna) on a gimbal that can rotate within specific elevation and azimuth directions. This simple setup allows the system to be kept at a relatively low level of complexity. However, it lacks durability scores as it includes bulky mechanical parts. As the interest in the topic grew, a new beam steering antenna type was introduced: the phased array antenna (Sometimes referred to as ESA, electronically steered antenna).

Furthermore, it is stated that currently deployed mechanically driven antennas in missiles are subject to be converted to the ESAs [1]. However, such antennas have a higher level of electrical design complexity in contrast to the mechanically steered antennas because they usually require individual control circuitry for each antenna cell that adjusts the amplitude and phase of the cell. Phase control over each antenna cell enables the user to focus the overall array beam in a specific desired direction, and this topology eliminates the need for a sizeable reflective dish to achieve high gain.

ESAs can achieve beam-steering via various methods, including analog and digital beamforming. Firstly, in analog beamforming, each antenna cell's excitation or receiving vector is created via dedicated beamforming hardware, i.e., VGA (Variable Gain Amplifier) and phase shifter ICs. In contrast, digital beamforming does not require additional hardware to tweak the element vector and achieve beam-steering, but it needs dedicated T/R (transmit-receive) ICs for each antenna cell. This method applies the element vector to the transmitted/received signal in the digital domain. In addition, DBF (Digital Beam Forming) has the ability to have multi-beam steering as the beamforming is carried out purely in the digital domain. However, this process increases the computational cost significantly compared to a single T/R module solution of analog beamforming. There is a trade-off between analog beamforming's poor durability and reliability problem and digital beamforming's high computational

cost. Due to this situation, both topologies are still used widely in the market depending on the platform's purpose and the end-user's needs.

For either of these architectures, the phased array antenna requires fine adjustments of its control parameters, in other words, a calibration routine before use, because the accurate alignment of relative phases of each antenna cell plays a significant role in the antenna's overall performance. Differences in fabrication processes and other environmental factors such as temperature changes, moisture exposure, and semiconductor aging cause deviation from the desired response of the semiconductor devices [2] [3] [4]. This deviation emerges as an RMS error from the desired phase response for phase shifters. Also, the use of digital phase shifters introduces quantization error. On the other hand, apart from deviations caused by physical factors, another phenomenon that causes an undesired effect on the overall response of the array antennas is called the mutual coupling effect. Mutual coupling between individual antenna cells causes degraded performance on array response because re-radiation from neighboring antenna cells interferes with the desired antenna excitation[5]. This effect becomes significant when the antenna cells are laid out closer. Considering these error sources combined, it is crystal clear that there is a need for compensation, i.e., a calibration routine for all the errors resulting from the factors mentioned above [6].

There are numerous calibration methods for phased arrays, which mainly depend on the application. For most uses, single calibration at the fabrication and later sparsely repeated onsite calibration processes are enough, given that the antenna will not be susceptible to a dramatic change in environmental conditions. For these cases, calibration is usually carried out in the anechoic chamber with a reference probe, and there are different methods to carry out the calibration process. After fabrication, onsite calibration may be necessary after shipment, integration, etc. For onsite calibrations, the most used methods include built-in reference antennas because of the lack of instrumentation in the operation field [7].

In this thesis, a calibration method is analyzed in depth for guided missiles with RF seekers that utilize ESAs. For guided missiles, RF seekers search for the target with

an RF signature and feed the related target information to the missile control algorithm. However, due to formerly mentioned error sources, the importance of the calibration process becomes significant, as it would directly affect the overall mission success. For most missile systems, the inventory may not be applicable to be calibrated frequently; in fact, the device may oblige to remain on standby for years. In that case, the alignment of the phased shifters would be disrupted. In addition, due to the nature of missile's mission, the device's calibration needs to be handled by itself. In other words, a self-calibration routine should be introduced [8]. Since the missile platforms are tightly populated in terms of hardware, there is not much space left for additional calibration hardware inside the missile. The method analyzed in this thesis focuses on two main points for the calibration; no extra space is introduced for the antenna, and the self-calibration can be done without human interaction and interrupting the overall mission.

In order to comply with the focuses mentioned above, two well-studied methods, namely, mutual-coupling and peripheral fixed probes, are combined. The mutual-coupling method requires little or no additional geometry for the antenna but requires individual T/R modules for each unit cell. In contrast, the peripheral fixed probes method requires additional geometry, an additional probe, to be used as a reference antenna. The proposed method uses two antenna cells as reference probes with a reference signal for calibration. Later, the overall relative phase and amplitude distribution are measured by coupling between reference elements and the rest of the phased array elements and successively measuring each element and comparing it with the reference signal. This way, the relative phase shifts between successive antenna cells can be measured, recorded, and checked. Comparing the recorded values with the LUT (Look Up Table), the deviations can be detected. In order to re-align the antenna cells, the proposed method uses remapping individual phase shifter responses to the so-called "new phase shifters". Later, for the beam steering, the remapped phase responses are used for relative phase shifts for the unit cells. In the analysis part, the performance of the proposed method is discussed in terms of sidelobe levels, steering angle, and main lobe magnitude.

1.1 Organization of the Thesis

This thesis aims to provide brief literature and industry research about missile guidance techniques, seeker architectures used for guidance, and antenna types included in seeker systems, which are inspected in detail, namely, the phased array antenna. Finally, four calibration methods for the phased array antenna are investigated in detail. Later, a new calibration method is proposed for the phased array antennas in guided missile systems which aims to achieve a self-calibration function for the guided missiles that are exposed to error sources.

Chapter 2 provides necessary information for the motivation for this study, starting from guidance methods for missiles, antennas used in semi-active radars, phased array antennas, properties of different semiconductors used in components of phased arrays, and error sources in semiconductors and phased array antennas.

Chapter 3 explains different calibration methods in the literature alongside the proposed hybrid calibration method.

Chapter 4 analyzes the proposed calibration routine, which combines the aforementioned methods to achieve self-calibration alongside no additional antenna geometry.

Chapter 5 concludes the overall study and ends with the references.

CHAPTER 2

LITERATURE REVIEW

2.1 Guidance Methods for Missiles

Modern cruise or ballistic missiles combine multiple guidance systems that are complementary to each other to achieve perfect intercept with the target of interest. These systems may include GNSS (Global Navigation Satellite System), RF seekers, IR (Infrared Radiation) seekers, and INS (Inertial Navigation System). RF seekers usually provide terminal guidance from these systems, which is best suited for the job. The other may not be accurate enough for dynamic targets such as ballistic missiles or fighter jets [9].

RF-guided missiles may use passive, semi-active, or active guidance methods. In passive systems, the radar only looks for the RF signature emitted from the target without additional illumination. Because of that, this method is best suitable for anti-radiation missiles whose targets are mainly strong RF emitters such as ships, planes, or ground radars. In the semi-active configuration, in other words, bi-static radar configuration, as seen in Figure 2.1, the radar uses reflected waves from the target as it is illuminated by an external source such as ground radar or fighter jet's radar. The semi-active homing is sometimes referred to as "all-weather guidance" since it is a reliable operation in most challenging conditions. This results in, modern cruise or ballistic missiles often being equipped with semi-active homing radars. In active homing, the missile radar can detect and illuminate the target without needing an external illumination source. However, due to the missile's restrictions regarding power and size, the acquisition capabilities in terms of range are generally handicapped, resulting in a shorter range of operation compared to semi-active radar configuration.

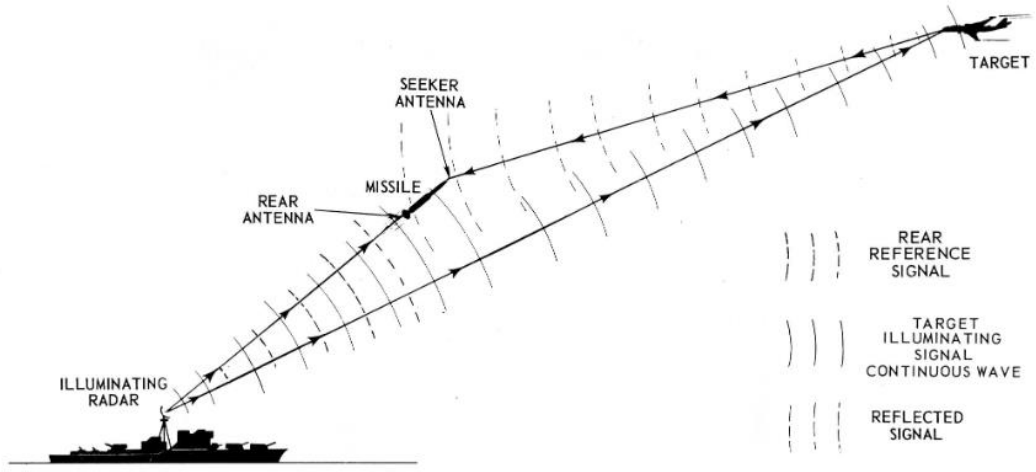

Figure 2.1. Semi-Active Guidance Configuration [10].

Given the reasons above, the semi-active configuration is the most deployed method for guided missiles.

2.2 Antennas for Semi-Active Guidance Systems

General hardware for semi-active radars consists of essential RF receiver parts: a receiving antenna, signal conditioning blocks, and the processor. Successively, the antenna takes the electromagnetic waves echoed from the target. In the signal conditioning part, the RF signal is filtered, amplified, and, if necessary downconverted to a predesigned intermediate frequency to be successfully sampled at the ADC. Finally, the received data is processed, and the target information is synthesized.

The design of signal conditioning and processor subsystems is usually straightforward as they only need to provide sufficient filtering, amplification, and certain SNR levels. However, the antenna subsystems play a leading role in overall radar performance. Because the target direction directly correlates with antenna pattern, which is the single key parameter to determining the target location.

The antenna beam must be directed towards the target to acquire an RF signature with as much SNR as possible to locate the target position. To achieve that, the

designs use two main topologies: mechanically steered antennas and electronically steered antennas (ESA).

Mechanically steered antennas achieve beam-steering by simply aligning the main beam direction of the antenna via a gimbal or pan-tilt device. However, ESAs are mechanically fixed, as they perform beam-steering via successively shifting phases of individual antenna cells. This allows it to focus the main beam in a certain direction. Being told, they both have pros and cons, which are explained in the following [11],

Mechanically steered antennas;

Pros:

- *High power handling capability is good, as they usually involve rigid metal dish antennas.*
- *Easier control of the direction in terms of elevation and azimuth thanks to the gimbal.*
- *The design of the overall antenna is straightforward.*

Cons:

- *Includes mechanically bulky parts and therefore susceptible to mechanical errors as they have electric motors in order to control the direction.*
- *Take up a large volume in a spatially limited environment, such as missiles.*
- *Failure of one element causes collapse in the overall antenna subsystem.*
- *Only one main beam is available, resulting in single target tracking, lacks multiple target tracking.*

Phased Array Antennas;

Pros:

- *Agile beam direction control is possible thanks to the fast phase shifting capabilities of MMICs (Monolithic Microwave Integrated Circuit).*
- *Failure of one or few elements usually acceptable with degraded performance.*
- *No moving mechanical parts, allowing it to be deployed in high velocity and high g platforms such as missiles.*
- *Multi-target tracking is possible with both analog and digital beamforming.*
- *System calibration can be done without human interaction, making it applicable for a non-human environment such as space or missiles on a mission.*

Cons:

- *Cost is relatively higher as compared to mechanically steered antennas, given the fact that semiconductor technology, which powers all critical components of the phased array, is still new and expensive.*
- *Control circuitry is very complex in both hardware and software aspects.*
- *Requires calibration of phases due to sensitivity of semiconductor devices to environmental conditions and aging.*

2.3 Phased Array Antennas in Radars

As explained in section 2.2, cruise missile and surface-to-air missile (SAM) radars usually utilize semi-active guidance. Therefore, most of the ESAs in missiles are receive-only antennas, meaning they do not have any transmitting hardware. In the following sections, receive only phased arrays, and their beam steering theory is explained.

2.3.1 Array Factor

Array theory suggests that geometrically related antennas contribute to the overall radiation pattern concerning their design parameters, such as the positioning of the antenna cells. From Balanis' Antenna Theory book, the most recognized and comprehensive literature source for antennas, the array factor for an MxN planar array that is aligned to the x-y plane is derived as [12]:

$$AF(\theta,\phi) = \sum_{m=1}^{M}\sum_{n=1}^{N} I_{mn} e^{j(m-1)(kd_x \sin\theta\cos\phi-\beta_x)} e^{j(n-1)(kd_y \sin\theta\sin\phi-\beta_y)} \quad (1)$$

Where I_{mn} is excitation amplitude of mn^{th} element, dx, dy are separations between antenna cells in x, y-directions, β_x, β_y are progressive phase differences between antenna cells in x, y directions, and θ, ϕ are spherical coordinates.

Array theory suggests that the radiation pattern of the arrays stems from the summation of the individual beam radiated by unit cells. In the radiation space, lobes are formed where the phase fronts of radiated waves interfere constructively and vice versa.

2.3.2 Beam Steering in Arrays

In order to maximize the magnitude of the array factor, the complex exponential terms in the array factor expression must be zero or multiples of 2π. In equation form;

$$\beta_x = kd_x \sin\theta\cos\phi + 2\pi m \,, m = 0, 1, 2, \ldots \quad (2)$$

$$\beta_y = kd_y \sin\theta\sin\phi + 2\pi n \,, n = 0, 1, 2, \ldots \quad (3)$$

Where β_x and β_y are progressive phase shifts between elements. If the beam is desired to align with certain θ_0 and ϕ_0 angles, the corresponding phase shifts have one solution given that frequency, and the separation of the elements are kept constant. However, when the separation of antenna cells is larger than $\lambda/2$, there are multiple solutions for θ and ϕ where the array factor has local maxima. In other

words, grating lobes start to occur. This phenomenon is rarely acceptable for phased arrays due to the need to point to one target simultaneously. Especially for radars, such undesired beams may result in wrong target acquisition, and the overall function of the radar may diverge.

A simplified beam-steering phased array schematic and steered beam is given in Figure 2.2.

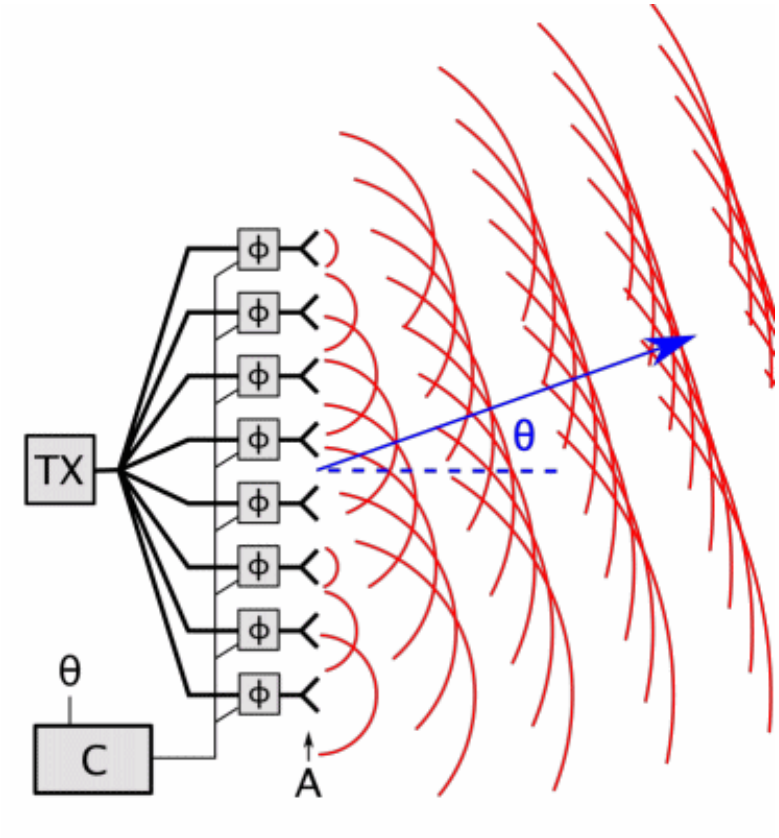

Figure 2.2. A transmitting phased array antenna diagram with its beam steered away from its boresight [13]

Although Figure 2.2 represents a transmitting array, since the antenna is a reciprocal device, the beam steering phenomenon is also valid for receiving phased arrays.

In addition to beam steering via phase manipulation, to further decrease SLLs in a phased array, an amplitude tapering can be applied. Most used distributions for amplitude tapering in phased arrays include Taylor distribution or binomial

distribution. However, amplitude distribution does not directly affect the calibration performance, it only affects the SLLs and radiation efficiency. In the Chapter 4 section 2.5, one tapered simulation case is included to demonstrate calibration performance with the presence of amplitude tapering (Figure 4.33).

2.3.3 Phase Shifter Technologies

Phase shifters ICs at high frequencies may utilize MMIC or MEMS (Micro ElectroMechanical Systems) technologies. However, when compared, MMIC has a much more developed infrastructure, and it is well studied and therefore has widespread use in the market. MEMS is relatively new and expensive, although it supports wider frequency bandwidths and provides higher linearity [14].

Similarly, MMIC technology has numerous developed processes, namely, GaAs devices, GaN devices, and Si-based devices. When compared, they have pros and cons depending on the application. A summary of the differences is given in Table 2.1.

Table 2.1. Performance Comparison of GaAs, GaN, and Si- Devices [15]

	GaAs	*GaN*	*Si-*
Frequency	Up to 250 GHz	Up to 30 GHz	Up to 3-4 GHz
Power	10 to 20 Watts	100s of Watts	1000s of Watts
Cost	1-2$ per Watt	4-5$ per Watt	1-2$ per Watt
Bandwidth	Narrow to Moderate	Wide	Narrow (>1 GHz) Wide (<1 GHz)
Linearity	Poor	Moderate	High

In the 1990's GaAs technology mostly replaced silicon for radars because of its wide frequency range, higher operating frequencies, and higher efficiency [16], [16]. On the other hand, GaN-based devices can handle higher energy densities; therefore, they are being used in power amplifiers. However, it is still new and pricey compared to GaAs, and there is room for more widespread use [15]. Therefore, it can be

concluded that most of the missile systems that are already deployed from the '90s to today still use GaAs technology for their seekers [16]. In addition, since GaAs devices lack higher operating powers, the radar systems using GaAs technology generally utilize semi-active or passive radar systems. Given the reasons above, in this thesis, the proposed method analysis is based on a commercially available Qorvo 6-bit phase shifter which uses GaAs pHEMT process [17].

2.3.4 Sources of Errors in Phased Arrays

Sources of errors in phased arrays can be scrutinized in three categories: random errors, drift errors, and systematic errors.

Random errors are present due to the nature of the elements in the system. They affect the performance in terms of phase noise and cannot be eliminated or compensated. However, their impact can be decreased by increased integration time and sophisticated signal processing techniques.

Drift errors emerge due to semiconductor misbehaving. Semiconductor devices such as amplifiers, phase shifters, or switches are susceptible to harsh environmental changes (temperature [18], humidity, and solar radiation [19]) and aging, and they respond to these effects by having degraded performance or complete failure. It can be seen from Figure 2.3 that semiconductors lose their reliability with aging.

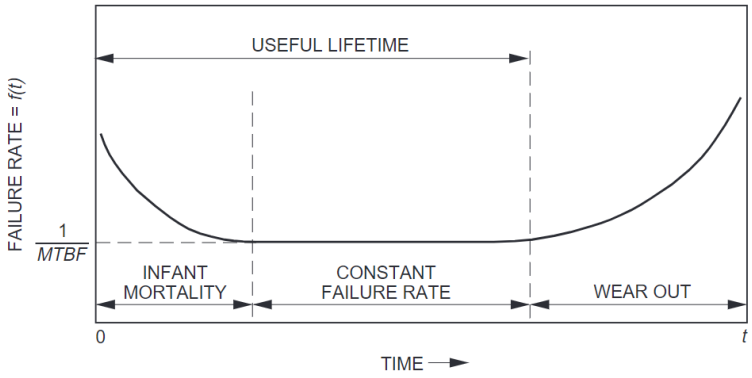

Figure 2.3. Semiconductor failure rate

Ohmic resistances in transistors (especially GaAs pHEMT) tend to increase due to the mentioned effects, and this results in increased insertion loss and changed phase response and amplitude responses. Although numerous research papers investigate the performance degradation of semiconductor devices, they mainly focus on insertion losses and failures but the phase response [20], [21]. Nevertheless, the phase performance degradation can be modeled considering VGAs in the I-Q paths of the receiver. Amplitude uncertainty cause phase deviation on the RF/IF paths, and this deviation reflects its effects as RMS (root-mean-square) error in the overall phase responses.

$$\sigma_{\phi} = \sqrt{\frac{\sum_{N}(\Delta\phi_n)^2}{N}} \qquad (4)$$

Where,

- $\Delta\phi_n$ is phase deviation of the n^{th} antenna element
- N is the antenna count in the array

Systematic or correlated errors are defined as non-altering errors on the DUTs (Device Under Test). In other words, the errors do not change between measurements at different times. In phased arrays, these errors include positioning errors of antenna elements, mutual coupling, the impedance mismatch between circuit components, and fabrication errors of the components. In addition, the physical structure of the platform that the antenna system is mounted on can affect the radiation pattern. Luckily, since these errors do not change between measurements, they can be compensated with proper calibration and alignment processes.

When all errors are considered, the performance of the phased array is affected. Imbalances of amplitudes and phases between antenna cells can result in reduced main lobe magnitude, increased SLL, and beam-pointing error [6].

CHAPTER 3

CALIBRATION METHODS OF PHASED ARRAYS ANTENNAS

Calibration routines exist to correct the mentioned errors caused by the antenna systems' nature. In the literature, the methods can be investigated in four main topics according to [22]. A complete picture of the errors, calibration methods, and the classification of the methods are given in Figure 3.1.

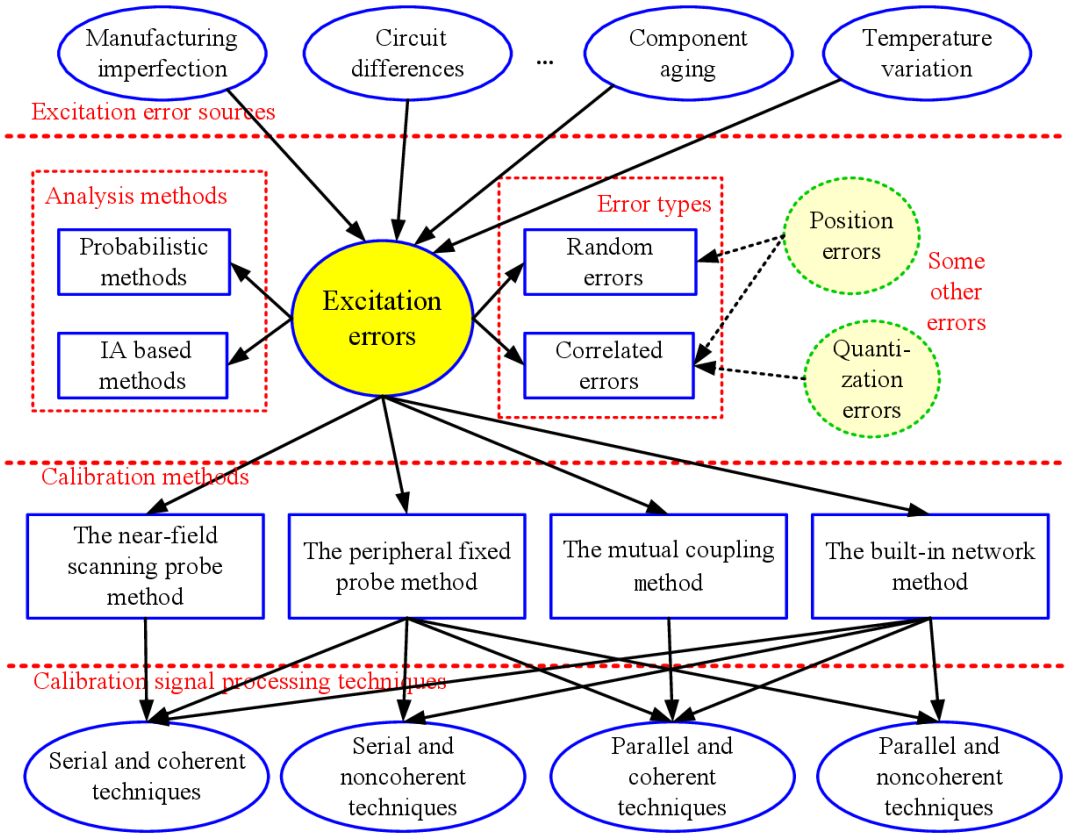

Figure 3.1. A complete scheme of the phased array antenna error sources and calibration methods[22]

As can be seen in Figure 3.1, there are four different techniques for calibration. In the following, each method is investigated in terms of hardware and applicability.

3.1 The Near-Field Scanning Probe Method

In this method, a reference antenna is placed in front of each antenna element while keeping relative positions unchanged. This method is widely used due to its accuracy and reliability. The procedure is straightforward, a mechanically controlled reference probe is cycled through each antenna element, and the measurement is taken via a VNA (Vector Network Analyzer). The key parameter that defines the accuracy of this method is the mechanically controlled probe's position. As long as the relative positions of each antenna element are the same, the measurement would not be compromised. The schematic for the method is given in Figure 3.2.

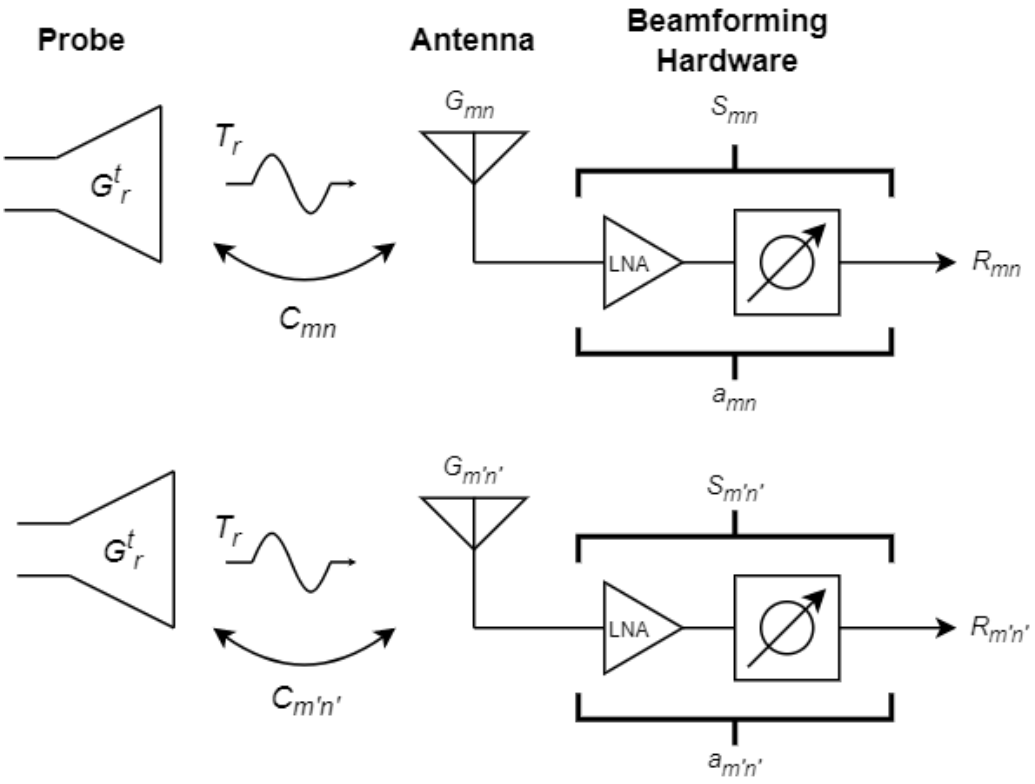

Figure 3.2. Schematic for near-field scanning probe method

The method uses the following formulas for mxn planar arrays:

$$R_{mn} = G_{mn}^{r}\, C_{mn,r}\, G_{r}^{t}\, T_{r}\, S_{mn}\, a_{mn} \qquad (5)$$

Where,

- R_{mn} The received signal from mn^{th} element
- G_{mn}^{r} , receive gain of the mn^{th} element
- $C_{mn,r}$, coupling ratio between reference antenna and mn^{th} element
- G_{r}^{t} , transmitting gain of the reference antenna
- S_{mn} , complex phase and amplitude setting for mn^{th} element
- T_{r} , transmitted signal by the reference probe
- a_{mn}, complex unwanted effects for mn^{th} element (to be calibrated).

Given that the relative positions with respect to each antenna element are the same, the coupling ratios are considered to be constant ($C_{mn,r} = C_{(m\prime n\prime),r}$ where the primed coordinates represent other elements). Therefore, the difference between each successive element can be found by,

$$\frac{R_{mn}}{R_{m\prime,n\prime}} = \frac{a_{mn}}{a_{m\prime,n\prime}} \qquad (6)$$

If the mn^{th}element is chosen as a phase reference for the other antenna cells; the calibration coefficients can be calculated by

$$K_{m\prime,n\prime} = \frac{a_{m\prime,n\prime}}{a_{mn}} \qquad (7)$$

Later, these coefficients for each antenna cell and each phase setting are applied via additional phase shifters for ABF (Analog Beam Forming) and complex multiplication in the digital domain for DBF.

The calibration steps are as follows:

1- Since only the phase difference is defining parameter for beam steering angle, one of the receiving elements is selected as a reference for the others.
2- All phase states for all antenna elements are measured via VNA, having amplitude and phase responses

3- The unwanted effects, a_{mn}, for each antenna element is calculated.
4- Finally, to compensate for unwanted effects, calibration coefficients $K_{m',n'}$, are multiplied by the received signal.

After calibration coefficients are calculated, the complex values are stored as LUT and used by the systems before operation.

Finally, the pros and cons of this method can be summarized as follows:

Pros:

- *Enables the user to properly carry out the first calibration of the antenna without any prior characterization.*
- *Since the ratios are considered for the calculation of coefficients, the effect of the reference antenna cancels out.*
- *The calibration routine takes into account all of the systematic errors.*
- *The far-field pattern can be synthesized using near-field measurements.*

Cons:

- *The calibration equipment is very mechanically bulky and expensive.*
- *Mechanical accuracy is the critical parameter for proper calibration.*
- *The method is most suitable for factory calibration; in-field calibration is not preferred.*
- *Overall calibration routine takes a long time, especially for large arrays*
- *Self-calibration is not possible.*

3.2 Peripheral Fixed Probes Method

In the peripheral fixed probes method, as the name suggests, a spatially fixed probe, in other words, a reference antenna, is strategically placed near the AUT. Comparing the near field scanning probe method, the reference does not move, eliminating the complexity and bulkiness of mechanical control systems. The reference antenna is usually placed at the center of the array to maximize the couplings between antenna cells and the reference antenna. Since relative positions between the reference

antenna and the antenna cells are different, unlike near field scanning probes, the couplings of the reference and the antenna cells are different. For this method to be applicable, the AUT should be calibrated beforehand. Later, couplings between the peripheral probe and the antenna cells are measured and recorded by sequentially exciting each antenna cell. After this step, the measurement is repeated and compared with initial calibrated values when the user wants to recalibrate the antenna. The related schematic of the method is given in Figure 3.3.

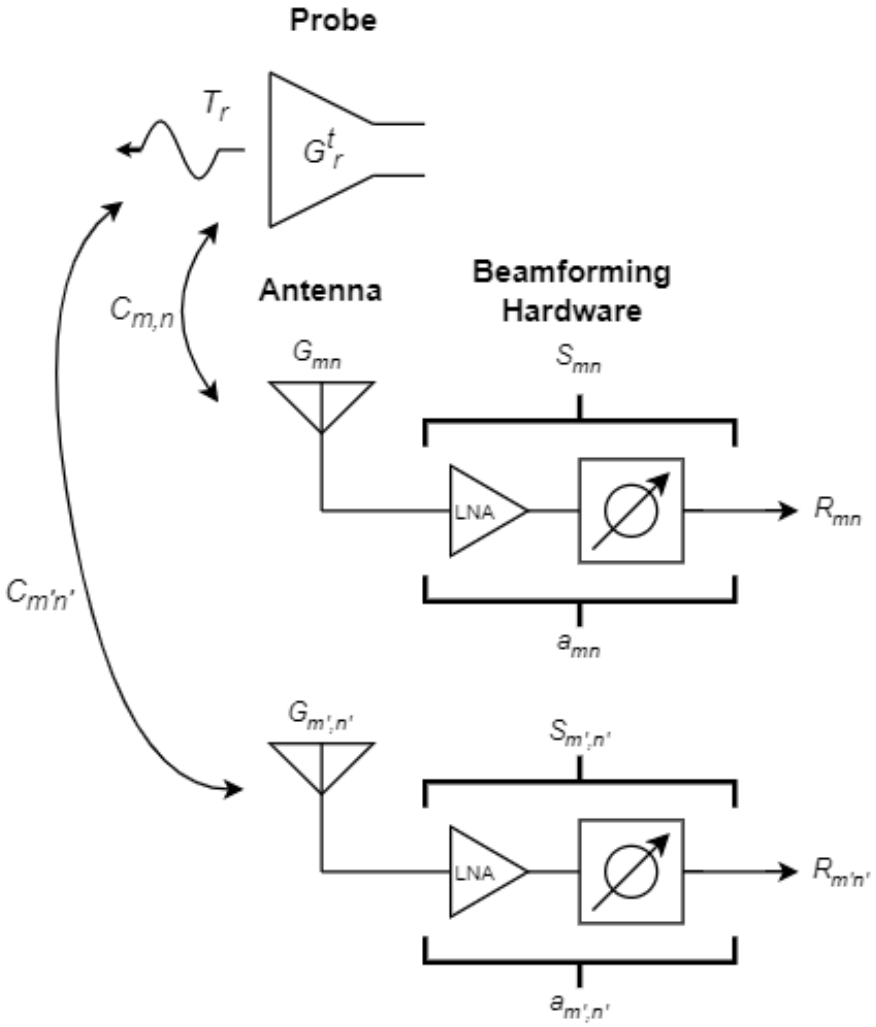

Figure 3.3. Schematic of the peripheral fixed probes method

The formulation is nearly the same as the near-field probes method, but the couplings between the reference and the antenna cells are different,

$$R_{mn} = G_{mn}^{r}\, C_{mn,r}\, G_{r}^{t}\, T_r\, S_{mn}\, a_{mn} \quad (8)$$

Where,

- R_{mn}, received signal from mn^{th}element
- G_{mn}^{r} , receive gain of the mn^{th}element
- $C_{mn,r}$, coupling ratio between reference probe and mn^{th}element
- G_{r}^{t} , transmitting gain of the reference probe
- S_{mn} , complex phase and amplitude setting for mn^{th}element
- T_r , transmitted signal by the reference probe
- a_{mn}, complex unwanted effects for mn^{th}element (to be calibrated).

After taking ratios between successive elements,

$$\frac{R_{mn}}{R_{m'n'}} = \frac{C_{mn,r}\ a_{mn}}{C_{m'n',r}\ a_{m'n'}} \quad (9)$$

Here, since the antenna has a prior calibration, the antenna has no unwanted effects, therefore,

$$\frac{R_{mn}}{R_{m'n'}} = \frac{C_{mn,r}}{C_{m'n',r}} = LUT_{m'n'} \quad (10)$$

Having acquired coupling ratios between each element, the user can calibrate the antenna whenever needed. If mn^{th} antenna is chosen as the reference antenna, the measured signals are compared with the LUT, and effects for the other antennas can be determined and later compensated via analog or digital techniques.

Calibration steps are as follows:

1- At the factory, initial calibration is carried out via a near-field scanning probe; later, coupling ratios between the peripheral antenna and the rest of the array are calculated and stored in LUT.
2- While in the field, relative couplings are calculated again and compared with the LUT. Differences are calculated as calibration coefficients.
3- Calibration coefficients are applied to each antenna element.

The pros and cons of this method can be summarized as follows:

Pros:

- *Enables user to carry out in-field calibration.*
- *Parallel calibration alongside the mission is possible.*
- *It does not require bulky mechanical parts.*
- *The change of characteristics of the peripheral probe does not affect the calibration as they cancel out.*
- *Self-calibration routine can be implemented.*

Cons:

- *The overall antenna geometry is increased.*
- *A prior calibration is required before carrying out peripheral probe calibration.*
- *The dynamic range of the receive antennas may become a problem in a large array due to the relative location of the probe being different for each antenna element.*

3.3 The Mutual Coupling Method

The mutual coupling phenomenon in antenna arrays stems from the array geometry usually packed with spatially close unit cells and dielectric substrates. Since the antennas are resonant devices, neighboring cells' radiation couples to other neighboring antenna cells when excited at the resonant frequency. This results in 'ghost excitation' in adjacent elements and eventually causes re-radiation from successive antenna cells. While some of the excitations from neighboring elements are re-radiated, a part of it is coupled to the antenna port. This method exploits this phenomenon to characterize the array. First proposed by H.M. Auman et al. [23], mutual coupling calibration enables antenna systems to be calibrated with no other geometry or prior calibration. However, this method requires individual T/R

modules behind each antenna element despite superiority over other methods. Figure 3.4 shows a simplified schematic and signals for mutual coupling calibration.

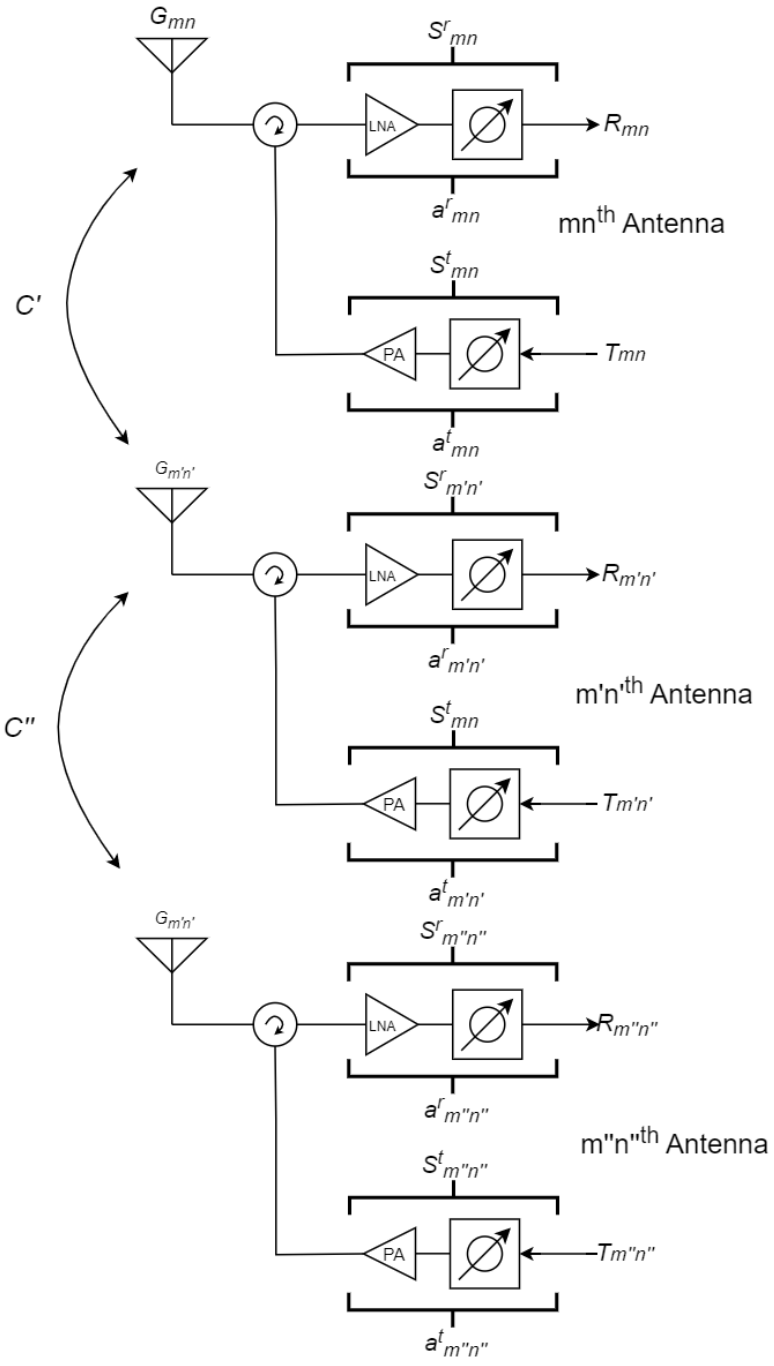

Figure 3.4. Schematic of mutual coupling method

The formulation of the mutual coupling method for receiving calibration is as follows:

$$R_{mn} = G^r_{mn}\, C'\, G^t_{m'n'}\, T_r\, S_{mn}\, a_{mn} \quad (11)$$

$$R_{m''n''} = G^r_{m''n''}\, C''\, G^t_{m'n'}\, T_r\, S_{m''n''}\, a_{m''n''} \quad (12)$$

Where,

- R_{mn} and $R_{m''n''}$, are received signals from mn^{th} and $m''n''^{th}$ element
- G^r_{mn} and $G^r_{m''n''}$, receive gain of the mn^{th} and $m''n''^{th}$element
- C', coupling ratio between $m'n'^{th}$antenna and mn^{th} element
- C'', coupling ratio between $m'n'^{th}$antenna and $m''n''^{th}$ element
- $G^t_{m'n'}$, transmitting gain of the $m'n'^{th}$ antenna
- S_{mn} and $S_{m''n''}$, complex phase and amplitude setting for mn^{th} and $m''n''^{th}$ element
- T_r , transmitted signal by the $m'n'^{th}$ antenna
- a_{mn} and $a_{m''n''}$, complex unwanted effects for mn^{th} and $m''n''^{th}$ element (to be calibrated).

The ratio of the received signals is the calibration coefficient for the neighboring elements:

$$\frac{R_{mn}}{R_{m''n''}} = \frac{C'\ a_{mn}}{C''\ a_{m''n''}} = K_{mn \to m''n''} \quad (13)$$

If the antenna geometry is uniform, that is, the structure is periodic, then $\angle C' \cong \angle C''$, thus, canceling out from the equation. Therefore, the ratios between received signals can quickly determine the calibration coefficient.

Pros:

- *Calibration can be done without any additional hardware.*
- *Enables user to carry out calibration whenever needed; in-field calibration is possible.*
- *The routine is inherently self-calibration capable.*
- *Suitable for calibrating large arrays.*

Cons:

- *Requires T/R module for each antenna element that can be simultaneously switched on/off.*
- *Element positioning should be uniform.*
- *Faulty elements disrupt the calibration sequence.*

3.4 The Built-in Network Method

In this method, individual transmission lines are assigned to each element, which is used as reference probes. Sometimes there can be individual calibration antennas for each antenna cell of the array which is to be calibrated. However, this geometry is not usually preferred due to the effect of calibration antenna on the antenna pattern, etc. Compared to the peripheral fixed probes method, the built-in network does not use antenna coupling for the reference signal transmission. Instead, the network is directly connected to the front end of the antenna via a switch. Therefore, this method does not cover antenna effects. The formulation is similar to the peripheral fixed probes method, the only difference being that there are transmission coefficients instead of coupling between the antennas. The schematic is given in Figure 3.5.

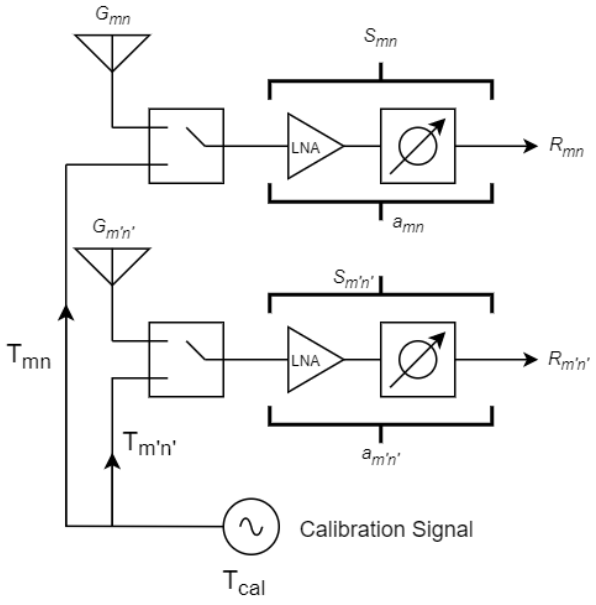

Figure 3.5. Schematic of built-in network method

Pros:

- *Suitable for in-field calibration.*
- *Inherently self-calibration capable.*
- *It does not increase the size of the antenna array.*

Cons:

- *Requires prior calibration at the factory.*
- *Includes additional hardware for each antenna.*

3.5 Comparison and Choice of the Calibration Methods

The choice of the calibration method depends mainly on two factors; antenna topology and the system's use case. Antenna topology is essential because specific calibration methods require additional hardware which cannot be populated in the antenna system. For example, the mutual coupling method only applies to T/R array antennas. When considering the use cases of the platforms, a self-aligning method may be necessary; for instance, human interaction is not usually possible for satellite or missile systems. Therefore, the designs should have the ability to calibrate themselves.

In this thesis, calibration for semi-active guided missile seeker antennas with self-alignment is aimed. Therefore, there are three main factors present. First, the antenna geometry should not be changed. Second, the antenna should have the self-alignment capability, and third, the antenna should be a receive-only array. For this purpose, it is decided that a hybrid method using mutual coupling and peripheral probes will be developed. In this hybrid method, two reference antennas are selected within the array. These antennas have a switch behind the antenna to switch between the reference and calibration modes. While calibration is in progress, the reference antenna emits a reference signal to the rest of the array, then, using mutual couplings between the reference antenna and the rest of the array, the individual characterizations of the antenna cells are extracted.

The schematic of the proposed hybrid method is given in Figure 3.6.

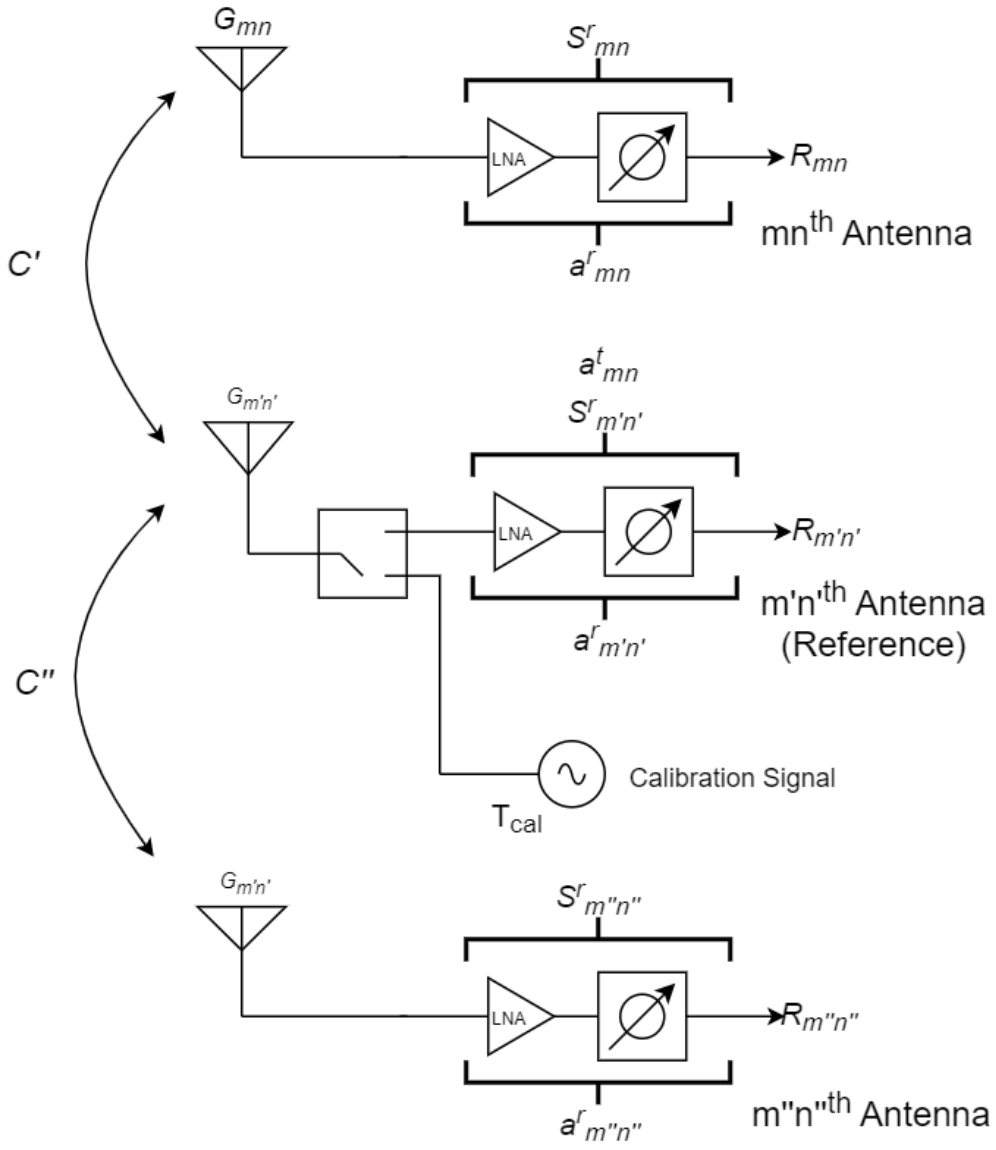

Figure 3.6. Schematic of the proposed hybrid method

This method will avoid the disadvantages of the mutual coupling and the peripheral fixed probes. Instead of having individual T/R modules for each antenna cell, only reference antennas will have a switch and a reference signal. Furthermore, thanks to switching action, there is no need for peripheral probes to be introduced, eliminating any alteration in antenna geometry. In the next chapter, the design, development, and analysis of the method are explained.

CHAPTER 4

ANALYSIS OF THE PROPOSED METHOD

Until this chapter, the problem is defined using the deduction method. In the final part, the proposed solution is investigated. MATLAB and CST Microwave Office programs are used for the analysis part to construct a sufficient simulation environment. Since a phased array antenna is a periodic structure, it is decided to utilize CST API using MATLAB to achieve automated operation and eased modeling process. MATLAB handles all parameter controls and algorithms for calibration and talks to CST API to realize corresponding simulations.

Design parameters are summarized in Table 4.1.

Table 4.1. Design Parameters for Phased Array Antenna

Parameters	*Values*
Design Frequency	10 GHz (X-Band)
Substrate	RO4003C(0.508mm)
Unit Cell Geometry(x-y)	18mm-15mm
Bandwidth	>100MHz
Array Size	8×4
Polarization	Linear
Spacing	$\lambda/2$

Design frequency is selected as X-band as is stated in Table 4.2, most suitable operation band for semi-active cruise missiles is X-band.

Table 4.2. Guidance techniques and corresponding operation parameters according to [24].

Guidance&Range	*Wavelength*	*Frequency*
Semi-active, up to 100 km	32 mm to 22 mm	9.375GHz to 13.63 GHz
Active, up to 15 km	22 mm to 8 mm	13.63 GHz to 37.5 GHz
Active, 1 to 2 km	8 mm to 3 mm	37 GHz to 100 GHz
Radiometric, passive	8 mm to 3 mm	37 GHz to 100 GHz

Bandwidth is set to be >100 MHz to cover up the search and acquisition functions.

As the substrate, Roger's Corporation's RO4003C with 508 um thickness is used as it supports X-band, and it is an industry-approved substrate which makes it widely studied and well-known.

Array size is set to be 8×4, making it asymmetric to investigate calibration performance in asymmetrical arrays further. Also, 32 elements phased array is sufficient for indicating beam-steering performance changes in the antenna radiation pattern.

The antenna cell's polarization is linear to keep the overall antenna design simple. Different polarization schemes are present for seekers; however, for this study's sake, only the calibration routine is targeted; therefore, validation of antennas with varying polarization schemes is left for future work.

The antenna spacing in the array is set to be $\lambda/2$ to avoid any grating lobes [25].

4.1 Design of Phased Array

4.1.1 Unit Cell

Before synthesizing the whole array, the unit cell should be configured. Using the MATLAB script, the parameters are optimized for the requirements defined above, and the final unit cell is synthesized. Scattering parameters and radiation patterns of the unit cell are given in Figure 4.4 and Figure 4.5. For the feed, cylinders are used to mimic a 3.5mm SMA Connector. Also, the stack-up information can be seen in Figure 4.2.

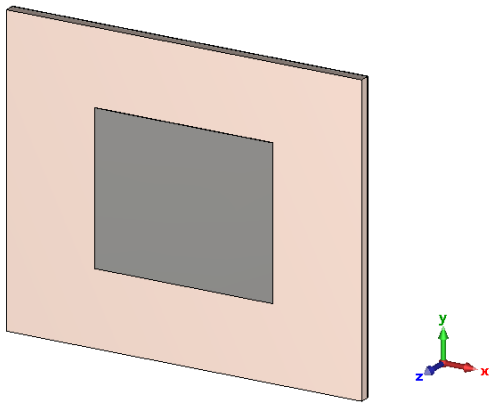

Figure 4.1. Unit cell perspective view

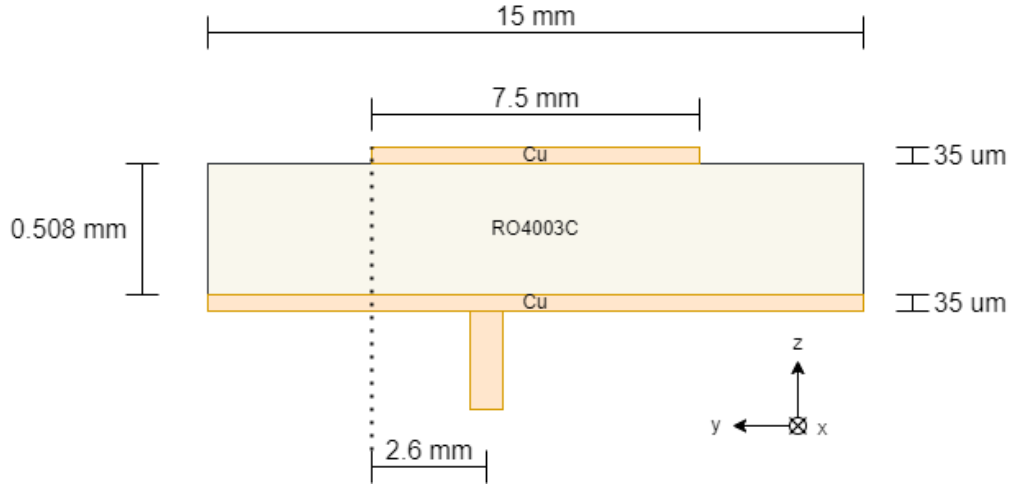

Figure 4.2. Stack-up of the unit cell

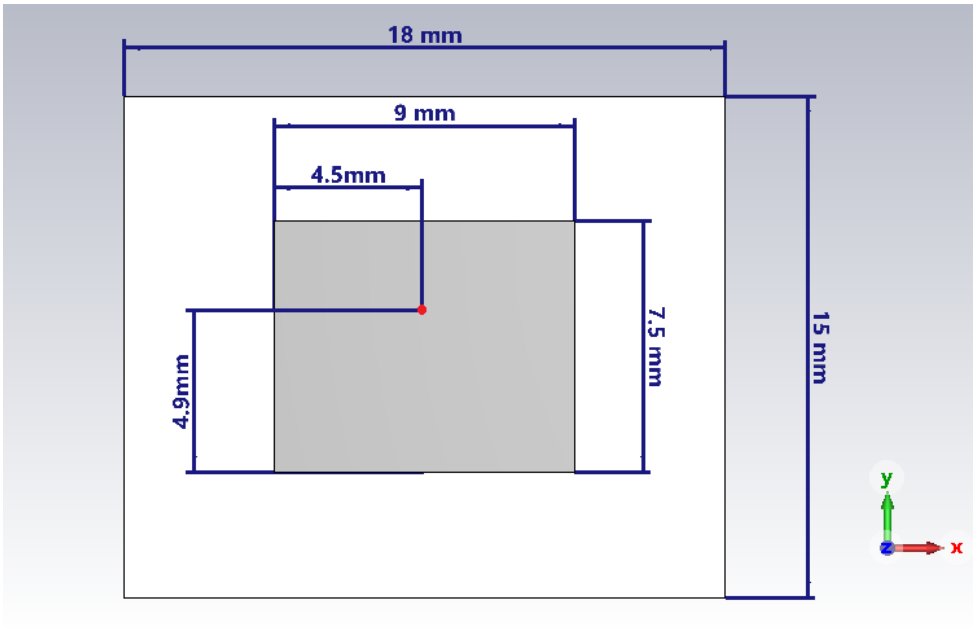

Figure 4.3. Patch dimensions and the feed location of the unit cell

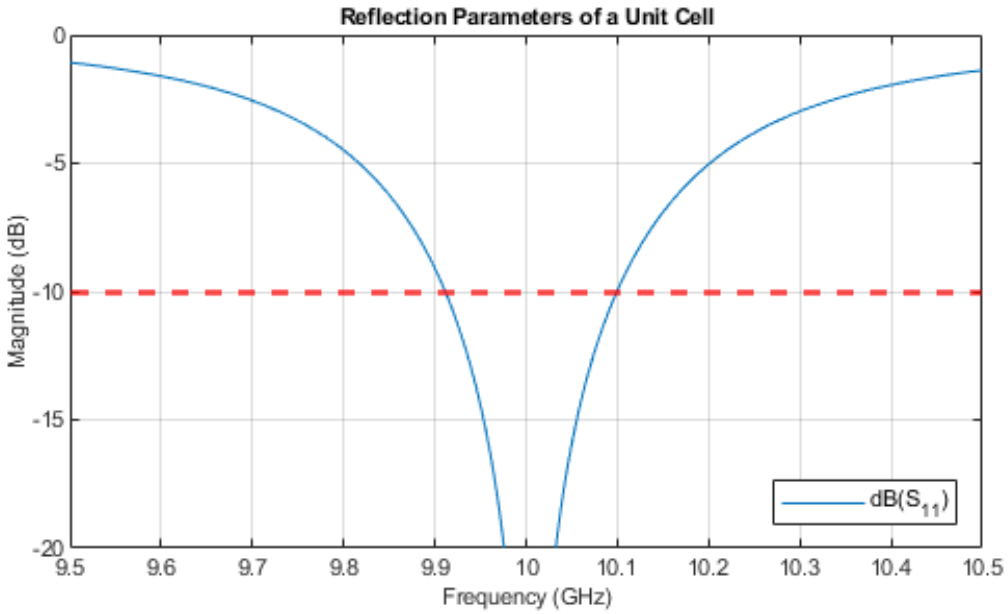

Figure 4.4. Reflection parameters of the unit cell (S_{11})

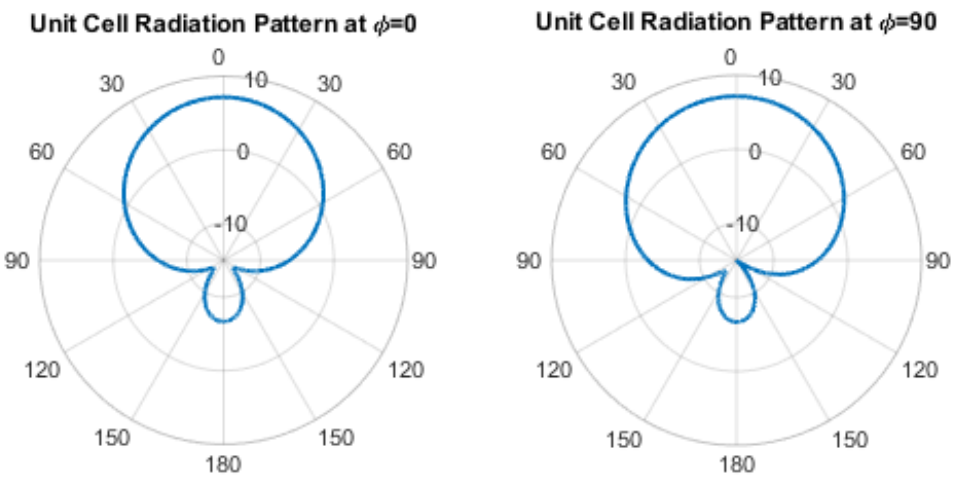

(4) (b)

Figure 4.5. The radiation pattern of the unit cell with two different cuts at $\phi = 0$ (a) and $\phi = 90$ (b)

A summary of the properties of the unit cell is given in Table 4.3.

Table 4.3. Synthesized unit cell properties

Property	*Values*
Beamwidth @10GHz	80°
Gain	7.15 dBi
Back lobe Level	-13.8 dB
Bandwidth	~200MHz

Having synthesized the unit cell, the array can be constructed.

4.1.2 Synthesizing The Array

Using the synthesized unit cell, it is time to create the array. With the help of MATLAB-CST API [26], the array is constructed with λ/2 spacing between the cells. The final array can be seen in Figure 4.6.

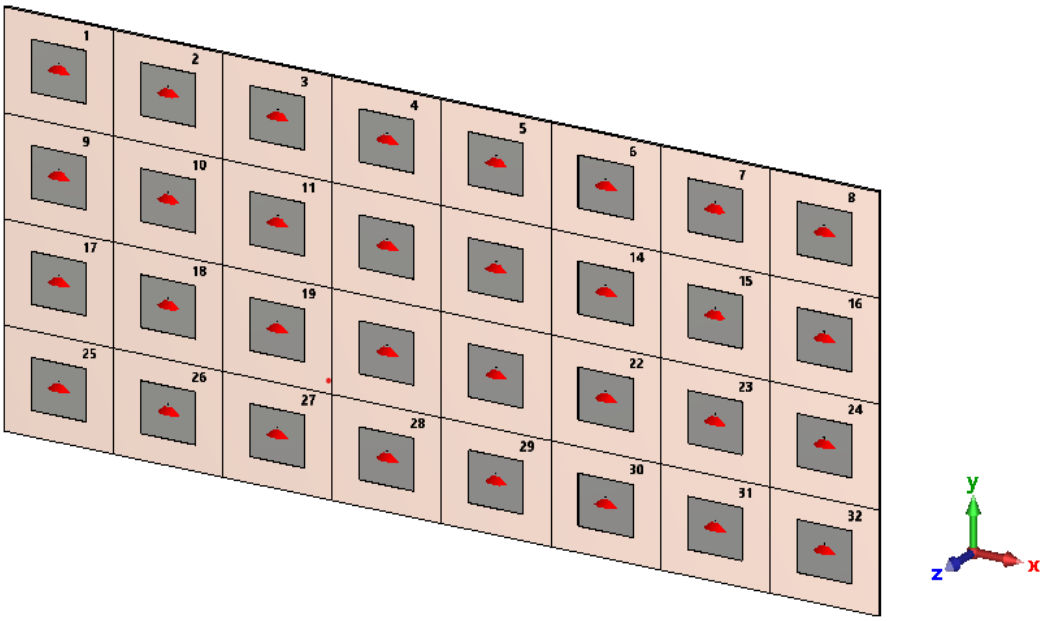

Figure 4.6. Synthesized array with 32 elements

Reflection parameters of the individual antenna cells show an operable region around 10GHz, even though mutual coupling slightly disrupts some of the responses (Figure 4.7)

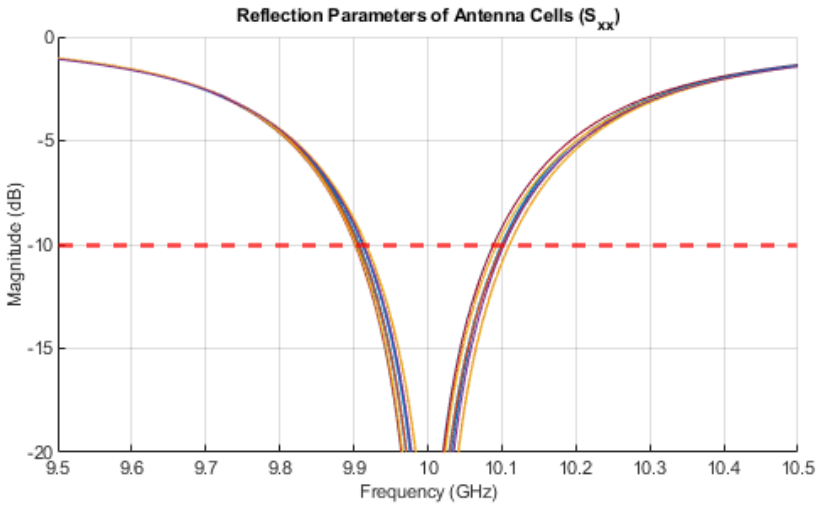

Figure 4.7. Reflection parameter of antenna cells (Sxx)

After validation of individual antenna performances, radiation patterns for different steering angles are investigated. For this purpose, the spherical angles θ and ϕ are swept individually, keeping one constant at 10 GHz, the center frequency. In Figure 4.8, different θ angles are swept up to 30 degrees to avoid grating lobes.

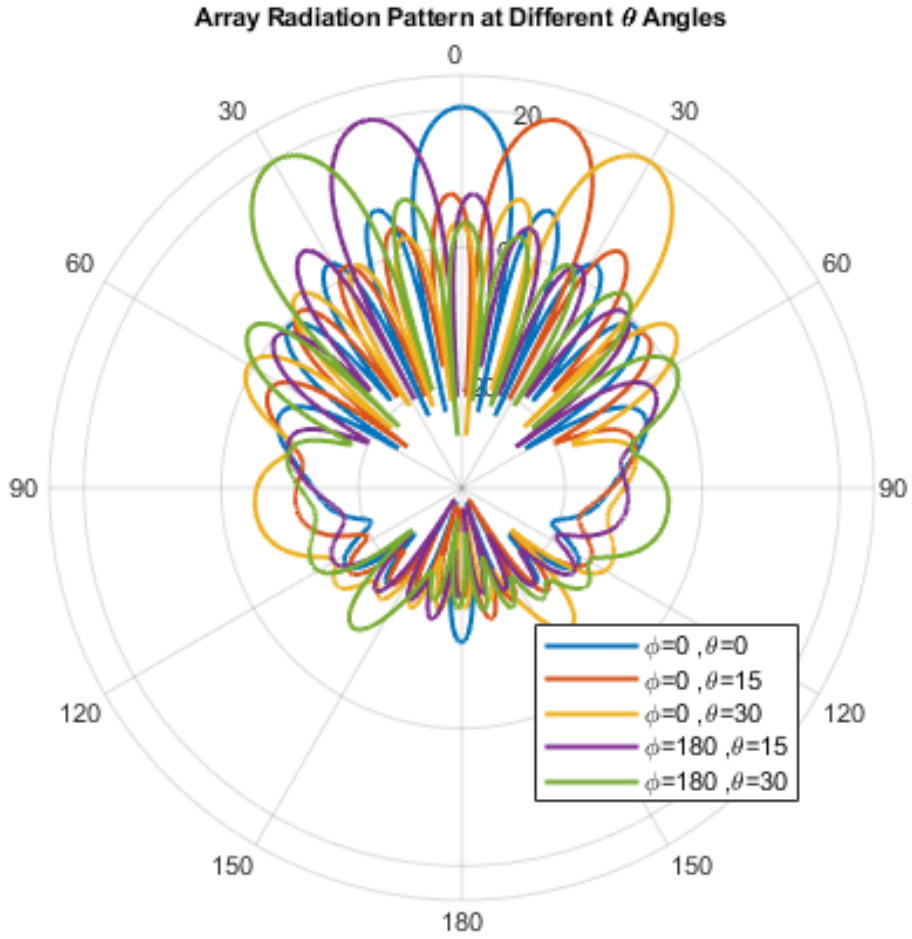

Figure 4.8. Radiation patterns at different θ angles in xz-plane cut

Table 4.4. Numerical results of Figure 4.8

Steered Angle (ϕ, θ)	*Gain*	*Beamwidth (3dB)*	*Side Lobe Level*	*Radiation Efficiency*
0°, 0°	20.4 dBi	10.6°	-13.2 dB	-0.40 dB
0°, 15°	20.2 dBi	11°	-12.5 dB	-0.41 dB
0°, 30°	19.7 dBi	12.3°	-12 dB	-0.48 dB
180°, 15°	20.2 dBi	11°	-12.5 dB	-0.41 dB
180°, 30°	19.7 dBi	12.3°	-12 dB	-0.48 dB

For the analysis of beam steering in ϕ angles, θ is fixed to 30 degrees, and ϕ is swept by 60-degree steps in Figure 4.9.

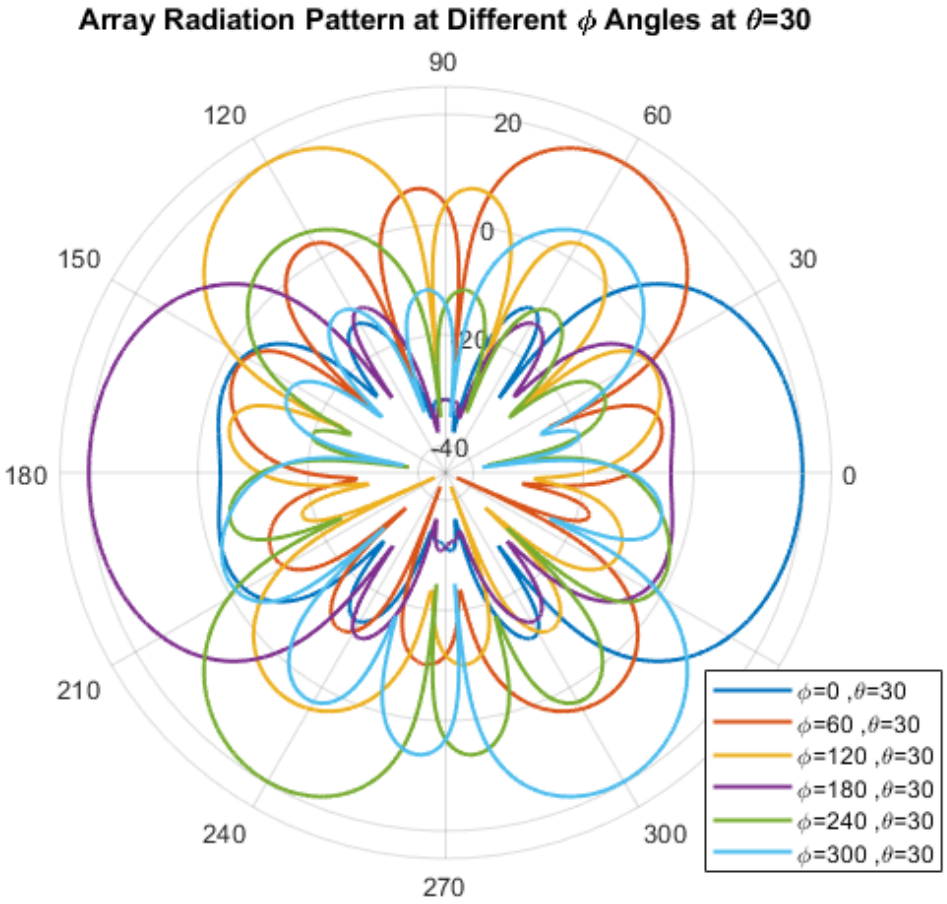

Figure 4.9. Radiation patterns at different ϕ angles in θ=30 cuts

Table 4.5. Numerical Results for Figure 4.9

Steered Angle (ϕ, θ)	*Gain*	*Beamwidth (3dB)*	*Side Lobe Level*	*Radiation Efficiency*
0°, 30°	19.7 dBi	47.9°	-21.6 dB	-0.48 dB
60°, 30°	19.7 dBi	24.7°	-13.0 dB	-0.39 dB
120°, 30°	19.7 dBi	24.3°	-13.0 dB	-0.39 dB
180°, 30°	19.7 dBi	24.3°	-13.1dB	-0.48 dB
240°, 30°	19.7 dBi	12.3°	-12 dB	-0.42 dB
300°, 30°	19.7 dBi	24.3°	-13.3 dB	-0.42 dB

The given phased array design aims to be used in receive only, analogously beam steered architecture.

Having acquired a working phased array design, it is time to analyze the calibration routine and its hardware aspects.

4.2 Analysis of Proposed Calibration Method

As described in previous chapters, two of the calibration methods are used in the proposed method in this thesis. The flow of the overall routine is given in the following sections for better understanding. Later, each step will be discussed in detail.

4.2.1 Simulation of the Array

First, the designed antenna is simulated sequentially at each port. This first step aims to obtain full 32 port s-parameters, i.e., couplings between all the antennas. Since the couplings of the antenna cells are to be used for calibrations, their magnitude plays a significant role in the overall performance of the calibration; in other words, to achieve certain SNR values for the calibration, the magnitudes of the couplings must be enough. In addition, the optimum coupling values must be determined to assign perfect reference antennas for the reference signal.

4.2.2 Assigning the Reference Antennas

The antennas that will be used for calibration are switched between receive-only mode, i.e., normal operation mode, and the calibration reference mode. To assign the most suitable reference antennas, the couplings of each antenna cell to another are analyzed. However, since the antenna geometry is asymmetric (8×4), with the help of empirical knowledge, the overall antenna geometry is divided into two sub-arrays which are 4×4 antenna arrays. One reference antenna will be assigned to each sub-

array, maximizing overall SNR for each antenna cell. Equation 14 shows the formulation for calculating the average couplings of each antenna cell.

$$(C_{av}^{n})_{dB} = 10log_{10}\left(\frac{1}{N-1}\left(\sum_{i=1}^{N} S_{in}^{mag} - S_{nn}^{mag}\right)\right) \quad (14)$$

Where,

- $(C_{av}^{n})_{dB}$ is the average coupling of n^{th} antenna to the rest of the sub-array in dB scale
- N is the antennas in the sub-array
- S_{in}^{mag} is the coupling magnitude between n^{th} and i^{th} antenna in linear scale

Furthermore, at least two reference antennas are required to calibrate every antenna cell, including the switched reference cells. Average coupling magnitudes are calculated to decide which antennas will be used for reference. Figure 4.10. shows that at antenna numbers 19 and 22, the average values are maximized for each sub-array, hence maximizing the average SNR for calibration signals. Assigned reference antennas and the overall antenna layout with sub-array geometry can be seen in Figure 4.11.

While assigning the reference antennas, minimum level of the coupling can be used as well. Since the utmost antennas relative to reference antenna will have the lowest couplings in the sub-array, measurement taken from those antennas may not meet the SNR levels required for the calibration. However, this approach would result in reduced sub-array size. Different approaches could give better results, but, in this study, average couplings are used to determine the reference antennas of the sub-arrays. In the section 4.3.3, further analysis on this topic is given.

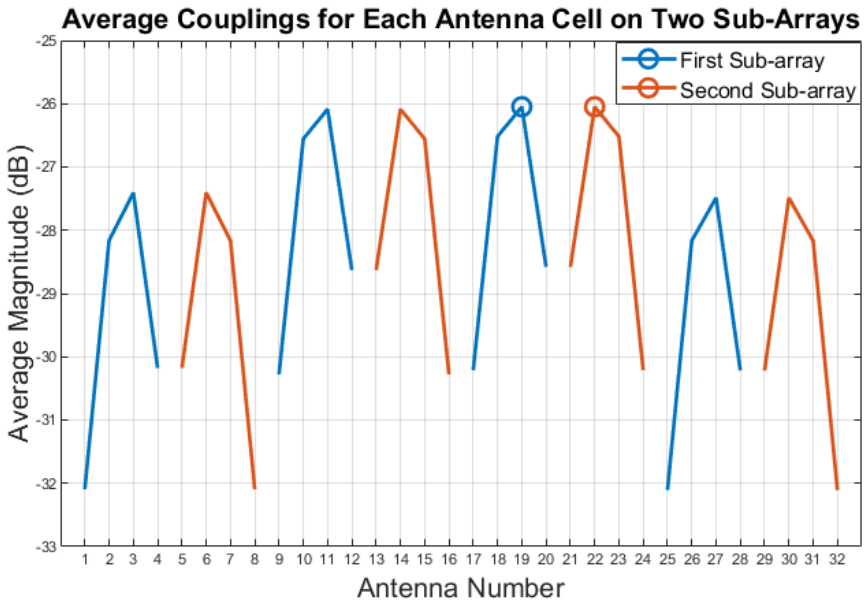

Figure 4.10. Average coupling magnitudes for each antenna cell on two sub-arrays

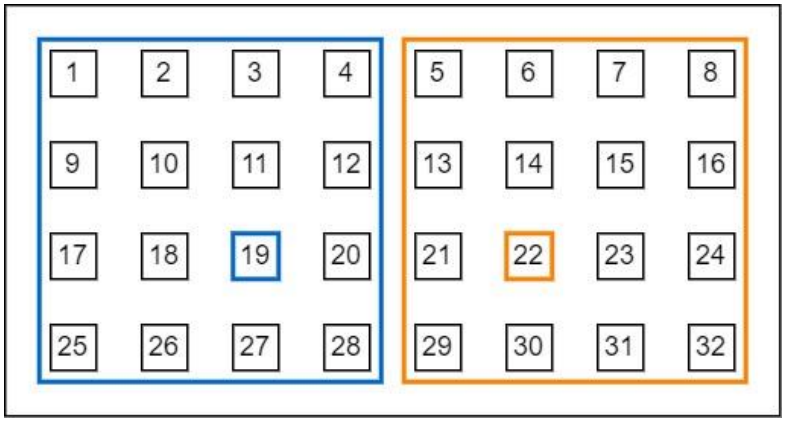

Figure 4.11. Antenna layout with assigned reference antennas and calibration sub-arrays

After assigning the reference antennas, the individual couplings and phase responses for both ($19^{th}$and 22^{nd} antennas) can be seen in Figure 4.12 and Figure 4.13. In the figures, couplings of the first sub-array are colored blue, couplings of the second sub-array are colored orange, and couplings of each reference antenna to the other are colored yellow and purple to be distinguished since they are in the other sub-array from each other.

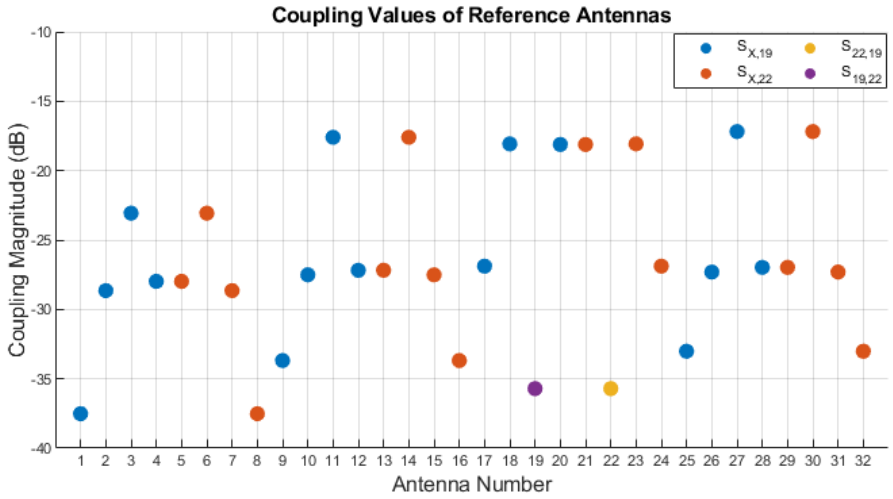

Figure 4.12. Coupling values from each antenna to reference antennas (19^{th} and 22^{nd})

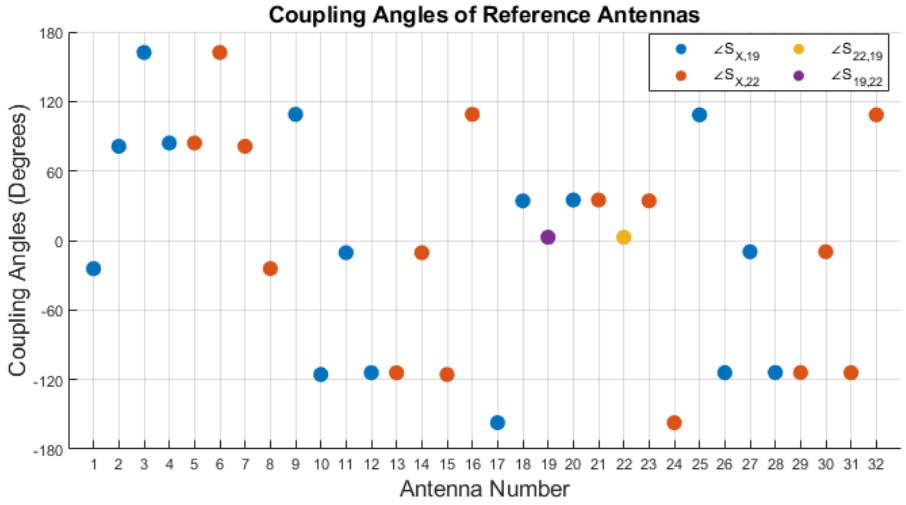

Figure 4.13. Coupling angles from each antenna to reference antennas (19^{th} and 22^{nd})

4.2.3 Error Modeling for Phase Shifters

As the topology suggests, each antenna cell has individual phase shifters. However, due to the aforementioned error sources in semiconductor devices and phase shifters discussed in Chapter 2, there is an inevitable RMS error in phase shifters and quantization errors. In this thesis, a commercially available X-band phase shifter is modeled to simulate real-life error effects, and company-provided s-parameter files

are used to reflect actual quantization error. After this step, to include drift and aging effects, a normally distributed phase error with an RMS error with a peak phase error of 40° is introduced to each step of the phase shifters. Overall steps for modeling the error flowchart are given in Figure 4.14.

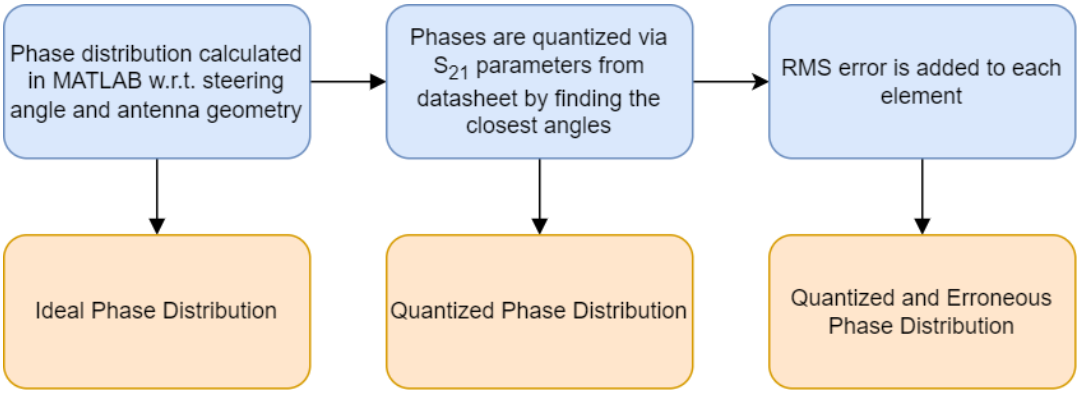

Figure 4.14. Steps of erroneous phase calculation

In addition to error scheme modeled above which is zero-mean and 40° peak phase error, additional error schemes are introduced with non-zero mean and dramatic peak phase errors. For this purpose, an additional 20° of mean error is added. For the dramatic case, the zero-mean peak RMS error is increased to 180°. In the results section the error cases are referred accordingly.

4.2.4 Correcting the Erroneous Phase Responses

The purpose of calibration is to correct undesired effects caused by phase deviations to proper ones. Regarding phased array beam steering, the most crucial parameters are the progressive phase shifts between the elements. The calculated progressive phase shifts must be present in each antenna cell to achieve a desired beam pointing angle. Otherwise, unwanted effects emerge, such as increased SLL, beam-pointing errors, and gain reduction.

To correct the disrupted responses, the phase responses of each element are measured by activating reference antennas and each other individually; later, in the ADC, the phase differences are measured. By cross-checking these differences by the LUT

created by the simulated quantized phase distributions, the erroneous phase values can be determined for each angle step in each phase shifter. After checking, in other words, characterizing all the phase shifters, the disrupted responses can be mapped to new control bits that give the desired phases, i.e., the algorithm changes control bits according to new responses. For example, if the phase difference between elements needs to be 30° for a particular beam steering angle, the control bits are readjusted with respect to their erroneous phases. A flowchart describing the algorithm is given in Figure 4.15.

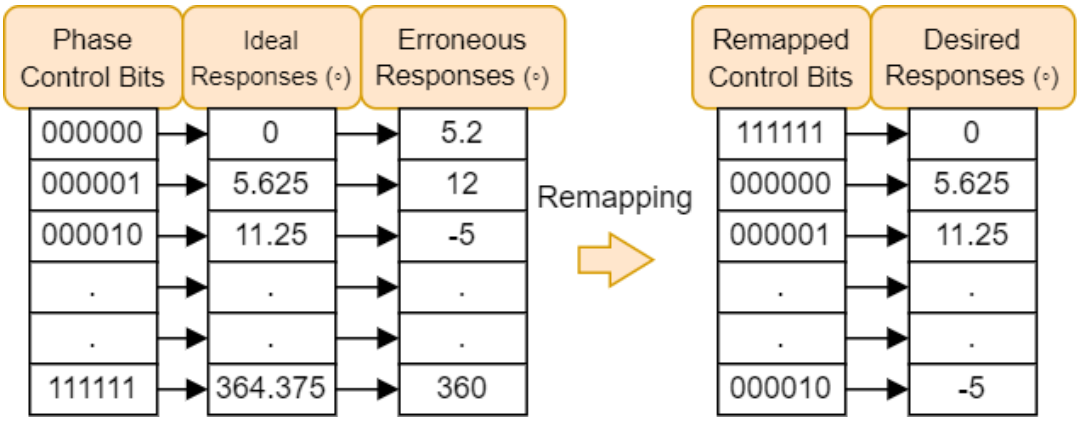

Figure 4.15. Remapping control bits to their new responses

After remapping and correspondingly using the new bits to adjust the phases, the desired phase distribution can be achieved. The averaged RMS errors for 1000 trials for erroneous and remapped phases for each phase distribution for different beam-steering angles are given in Figure 4.16. Note that the quantized RMS error is constant within the phase steps range, as the quantization steps do not change with respect to the phase distribution.

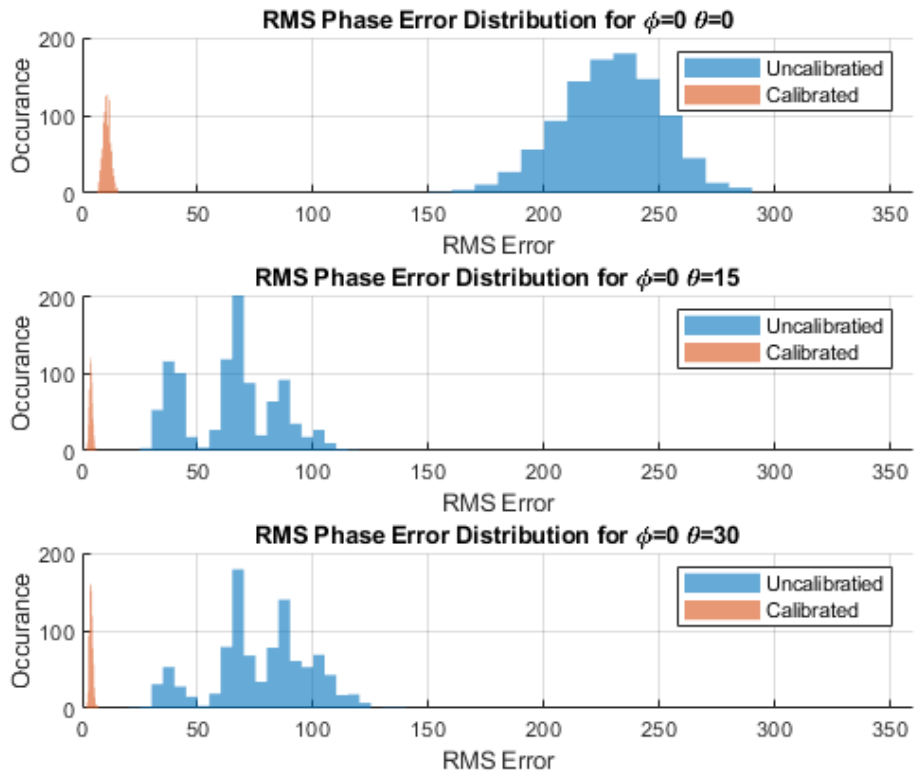

Figure 4.16. Monte Carlo simulations for uncalibrated and calibrated phase distributions for different phi and theta angles

The array's calibration performance is investigated in the next section after conducting the error and calibration model for the phase shifters.

4.2.5 Calibration of the Antenna Array

In order to investigate the calibration performance of the hybrid method, the structure is simulated with different beam-steering angles. For this purpose, first, θ is swept while keeping ϕ constant and vice versa. Figure 4.17 to Figure 4.27 show radiation patterns for different steering angles. Also, critical parameters are summarized in Table 4.6 to Table 4.16 correspondingly.

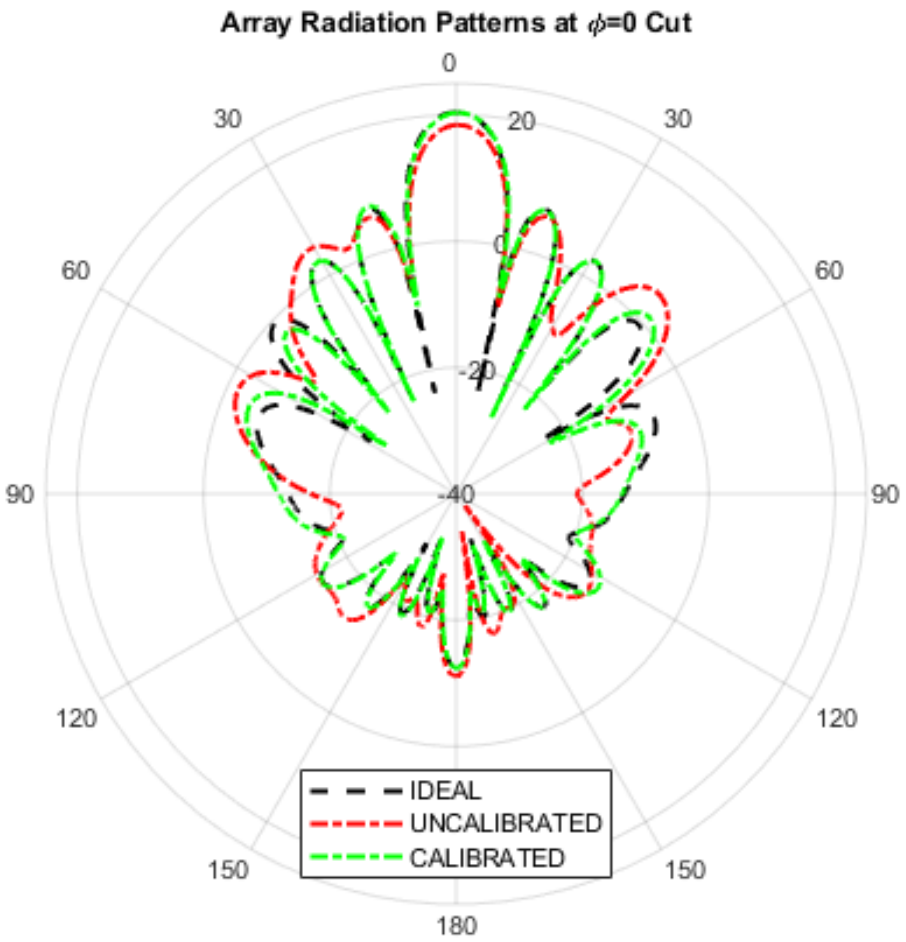

Figure 4.17. Radiation patterns for beam-steering angle $\theta_0 = 0^\circ$, $\phi_0 = 0^\circ$

Table 4.6. Numerical results for beam-steering angle $\theta_0 = 0^\circ$, $\phi_0 = 0^\circ$

	Main Lobe Direction (ϕ, θ)	*Gain*	*Beamwidth (3dB)*	*Side Lobe Level*
Ideal Case	0°, 0°	20.4 dBi	10.6°	-13.2 dB
Uncalibrated Case	0°, 0.3°	18.4 dBi	10.7°	-12.2 dB
Calibrated Case	0°, 0°	20.3 dBi	10.6°	-12.7 dB

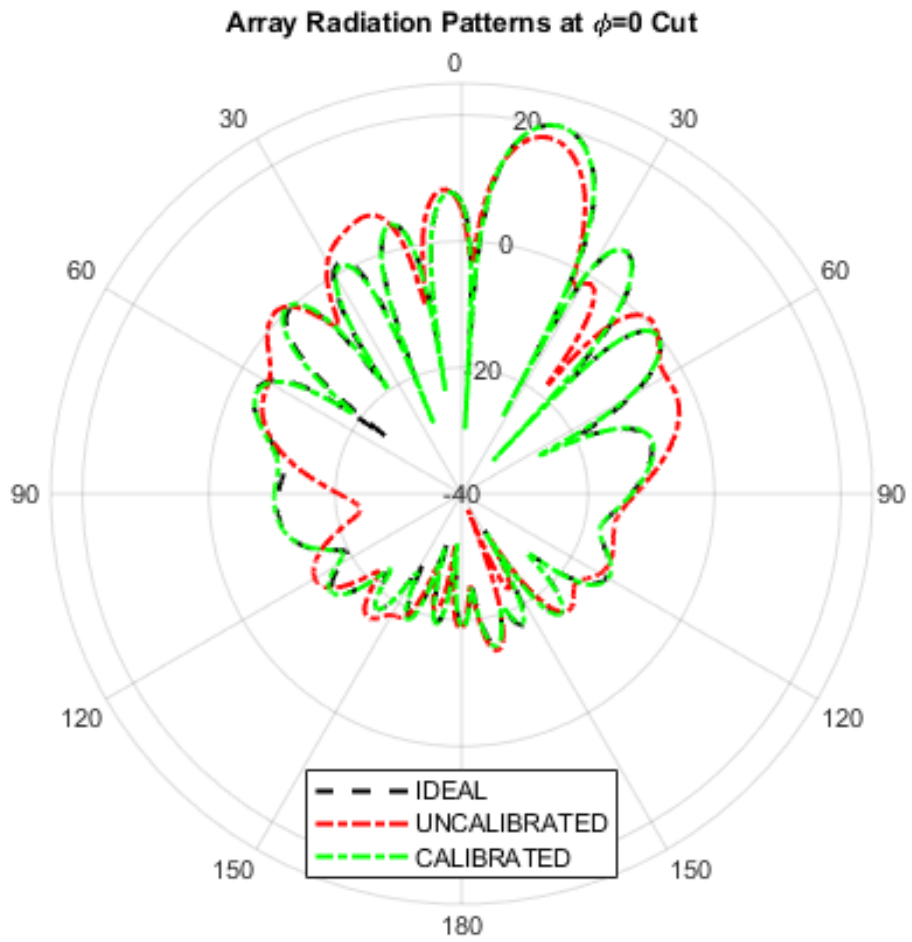

Figure 4.18. Radiation patterns for beam-steering angle $\theta_0 = 15^\circ$, $\phi_0 = 0^\circ$

Table 4.7. Numerical results for beam-steering angle $\theta_0 = 15^\circ$, $\phi_0 = 0^\circ$

	Main Lobe Direction (ϕ, θ)	*Gain*	*Beamwidth (3dB)*	*Side Lobe Level*
Ideal Case	$0°, 15°$	20.2 dBi	11°	-12.5 dB
Uncalibrated Case	$0°, 13.8°$	18 dBi	11.1°	-9.8 dB
Calibrated Case	$0°, 14.9°$	20.2 dBi	11°	-12.5 dB

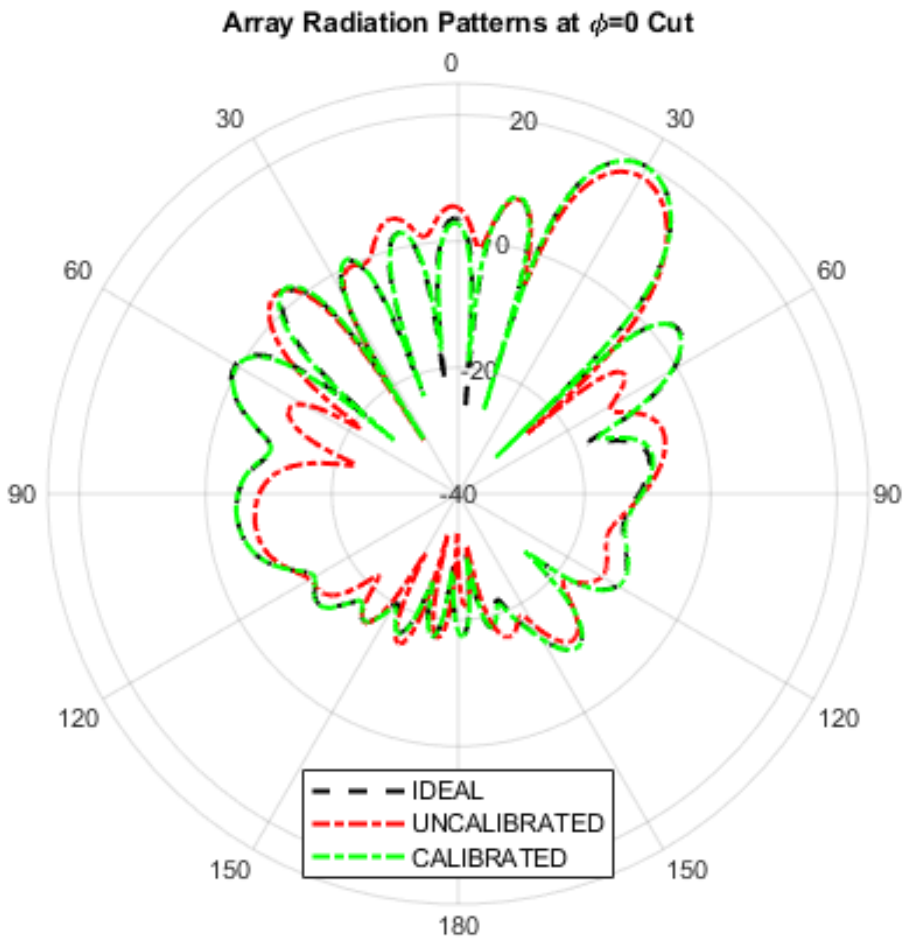

Figure 4.19. Radiation patterns for beam-steering angle $\theta_0 = 30^\circ$, $\phi_0 = 0^\circ$

Table 4.8. Numerical results for beam-steering angle $\theta_0 = 30^\circ$, $\phi_0 = 0^\circ$

	Main Lobe Direction (ϕ, θ)	*Gain*	*Beamwidth (3dB)*	*Side Lobe Level*
Ideal Case	$0°, 30°$	19.8 dBi	12.3°	-12 dB
Uncalibrated Case	$0°, 30.3°$	17.9 dBi	12.6°	-10.4 dB
Calibrated Case	$0°, 30°$	19.7 dBi	12.3°	-11.8 dB

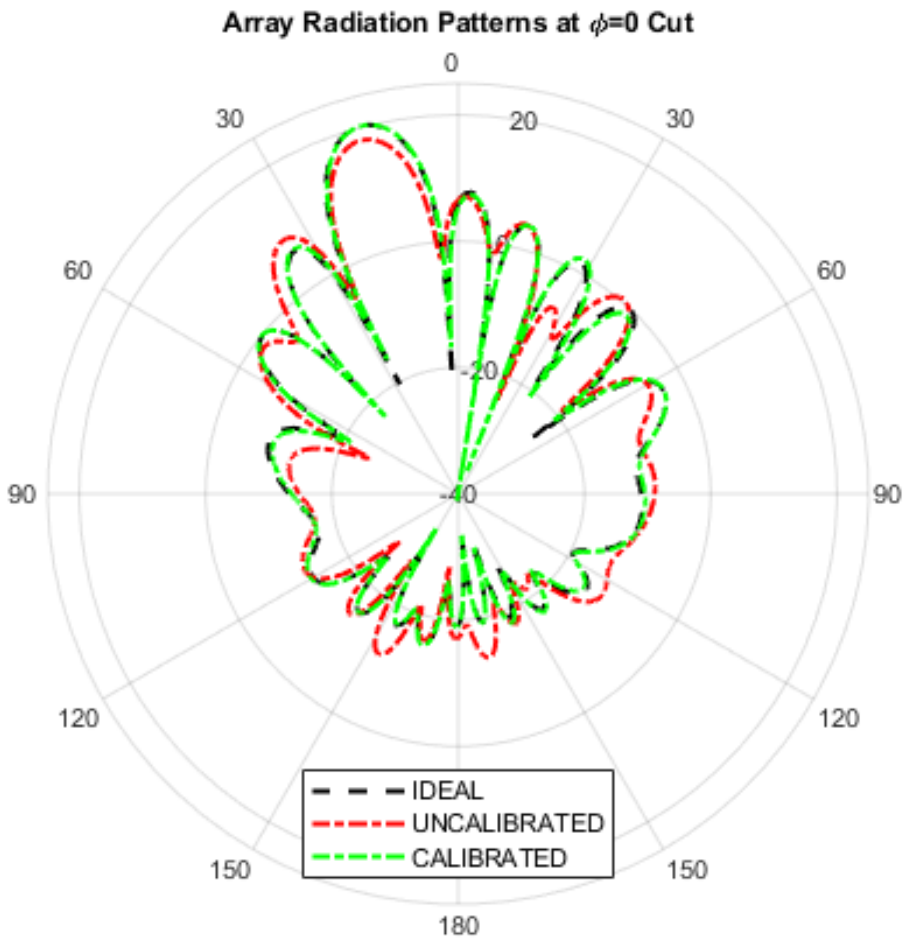

Figure 4.20. Radiation patterns for beam-steering angle $\theta_0 = 15^\circ$, $\phi_0 = 180^\circ$

Table 4.9. Numerical results for beam-steering angle $\theta_0 = 15^\circ$, $\phi_0 = 180^\circ$

	Main Lobe Direction (ϕ, θ)	*Gain*	*Beamwidth (3dB)*	*Side Lobe Level*
Ideal Case	180°, 15°	20.2 dBi	11.0°	-12.5 dB
Uncalibrated Case	180°, 15.6°	18 dBi	10.6°	-9.2 dB
Calibrated Case	180°, 14.9°	20.2 dBi	11.0°	-12.8 dB

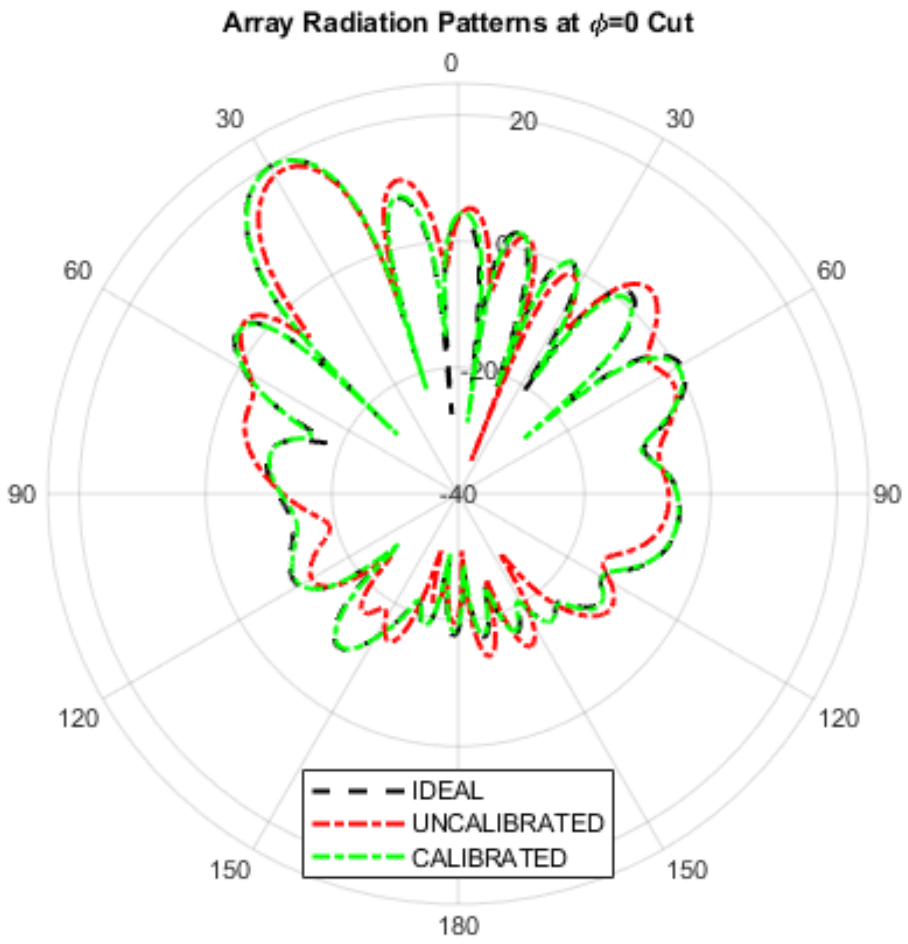

Figure 4.21. Radiation patterns for beam-steering angle $\theta_0 = 30^\circ$, $\phi_0 = 180^\circ$

Table 4.10. Numerical results for beam-steering angle $\theta_0 = 30^\circ$, $\phi_0 = 180^\circ$

	Main Lobe Direction (ϕ, θ)	*Gain*	*Beamwidth (3dB)*	*Side Lobe Level*
Ideal Case	180°, 30°	19.8 dBi	12.3°	-12.0 dB
Uncalibrated Case	180°, 28.7°	18.3 dBi	11.6°	-7.7 dB
Calibrated Case	180°, 30°	19.7 dBi	12.3°	-11.7 dB

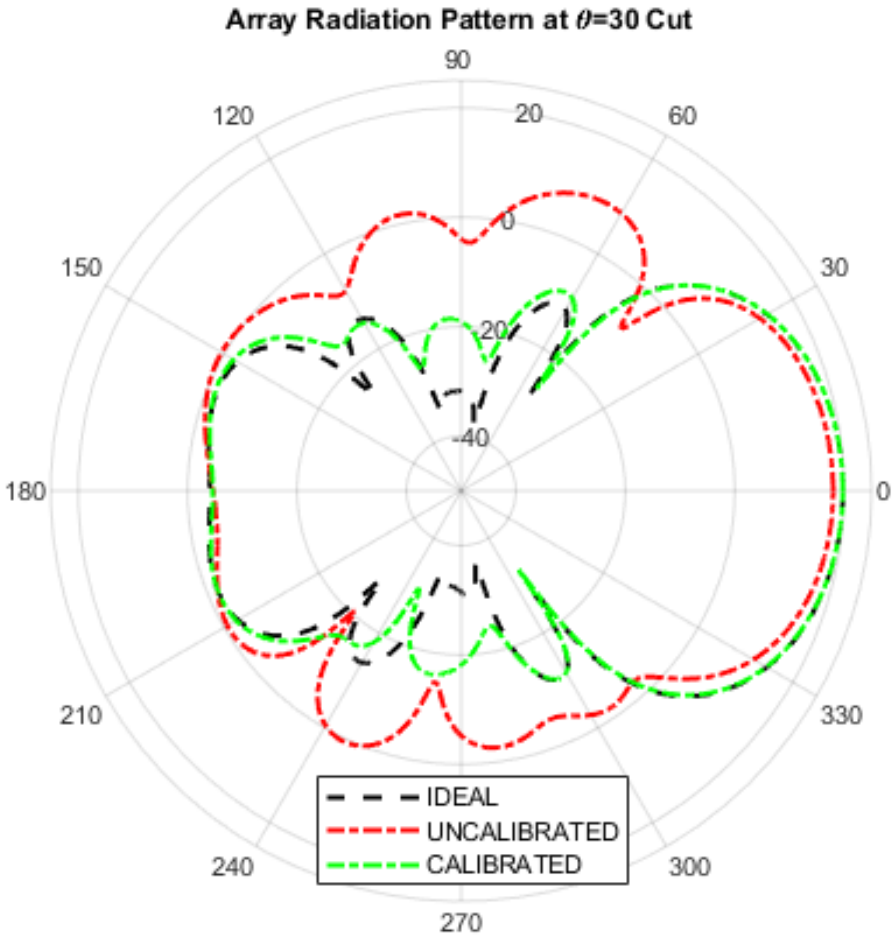

Figure 4.22. Radiation patterns for beam-steering angle $\theta_0 = 30^\circ$, $\phi_0 = 0^\circ$

Table 4.11. Numerical results for beam-steering angle $\theta_0 = 30^\circ$, $\phi_0 = 0^\circ$

	Main Lobe Direction (ϕ)	*Gain*	*Beamwidth (3dB)*	*Side Lobe Level*
Ideal Case	0°	19.7 dBi	47.9°	-21.6 dB
Uncalibrated Case	0.1°	17.9 dBi	47.5°	-9.1 dB
Calibrated Case	0°	19.7 dBi	47.9°	-21.2 dB

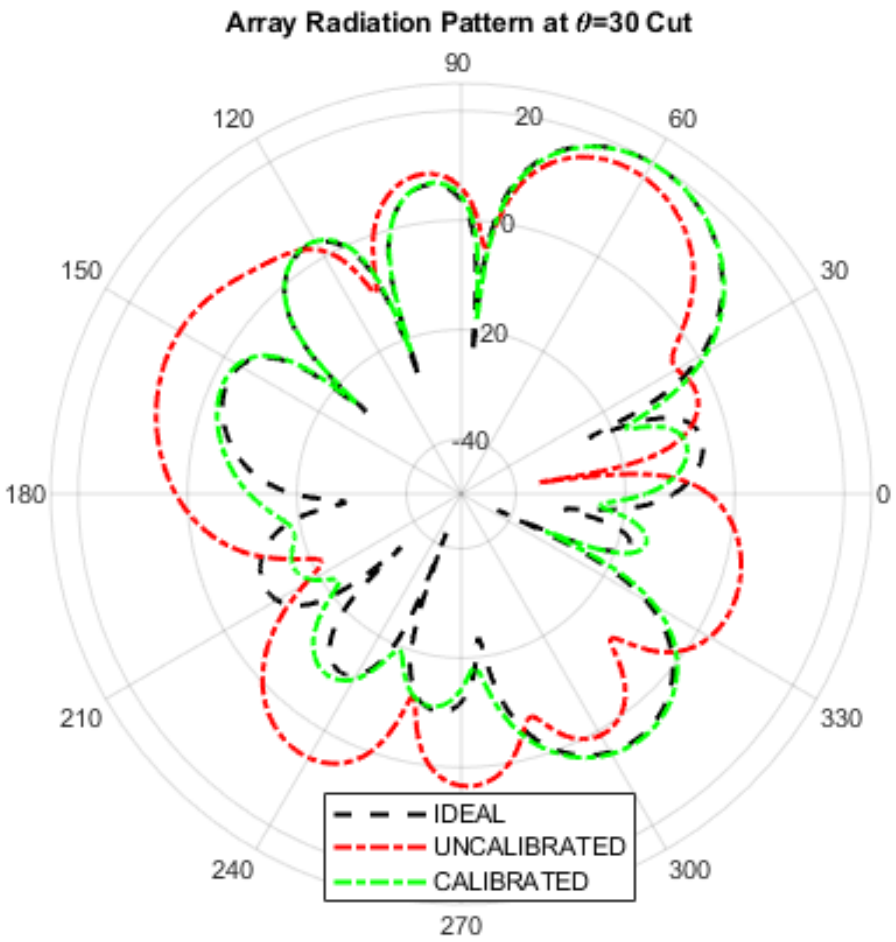

Figure 4.23. Radiation patterns for beam-steering angle $\theta_0 = 30^{\circ}$, $\phi_0 = 60^{\circ}$

Table 4.12. Numerical results for beam-steering angle $\theta_0 = 30$, $\phi_0 = 60$

	Main Lobe Direction (ϕ)	*Gain*	*Beamwidth (3dB)*	*Side Lobe Level*
Ideal Case	60°	19.7 dBi	24.3°	-13.0 dB
Uncalibrated Case	62.6°	16.9 dBi	22.0°	-7.5 dB
Calibrated Case	60°	19.7 dBi	24.3°	-12.7 dB

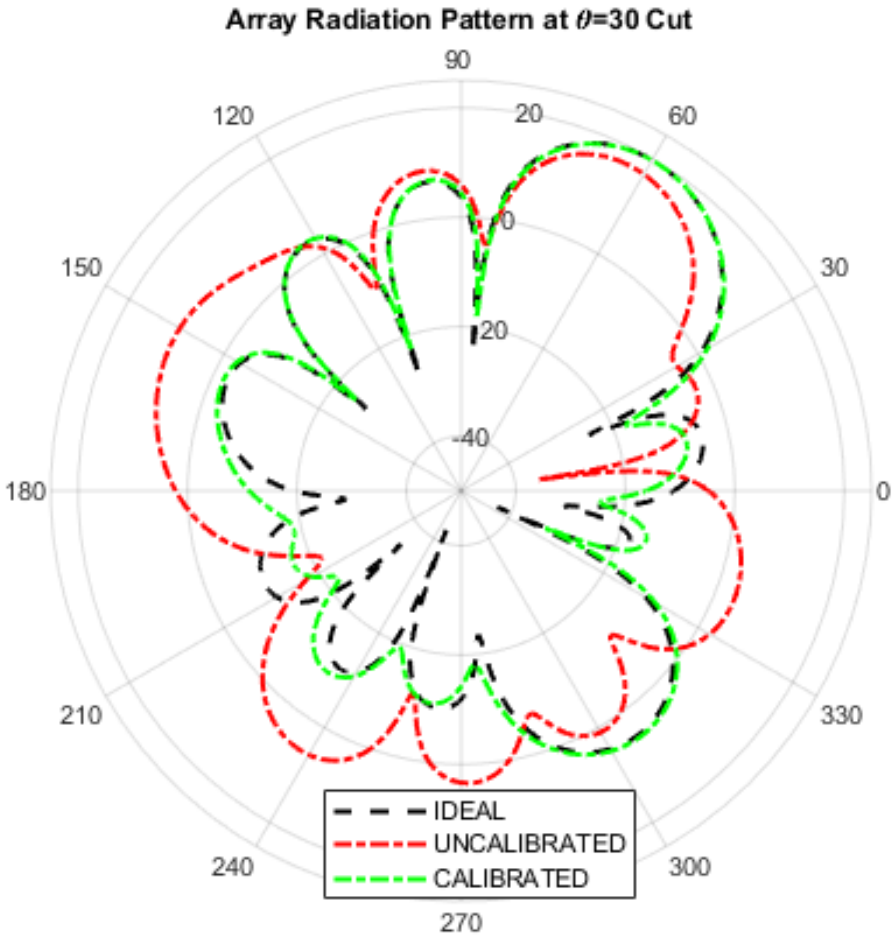

Figure 4.24. Radiation patterns for beam-steering angle $\theta_0 = 30^\circ$, $\phi_0 = 120^\circ$

Table 4.13. Numerical results for beam-steering angle $\theta_0 = 30^\circ$, $\phi_0 = 120^\circ$

	Main Lobe Direction (ϕ, θ)	*Gain*	*Beamwidth (3dB)*	*Side Lobe Level*
Ideal Case	120°	19.7 dBi	24.3°	-13.0 dB
Uncalibrated Case	119°	17.4 dBi	23.0°	-6.4 dB
Calibrated Case	120°	19.7 dBi	24.4°	-12.6 dB

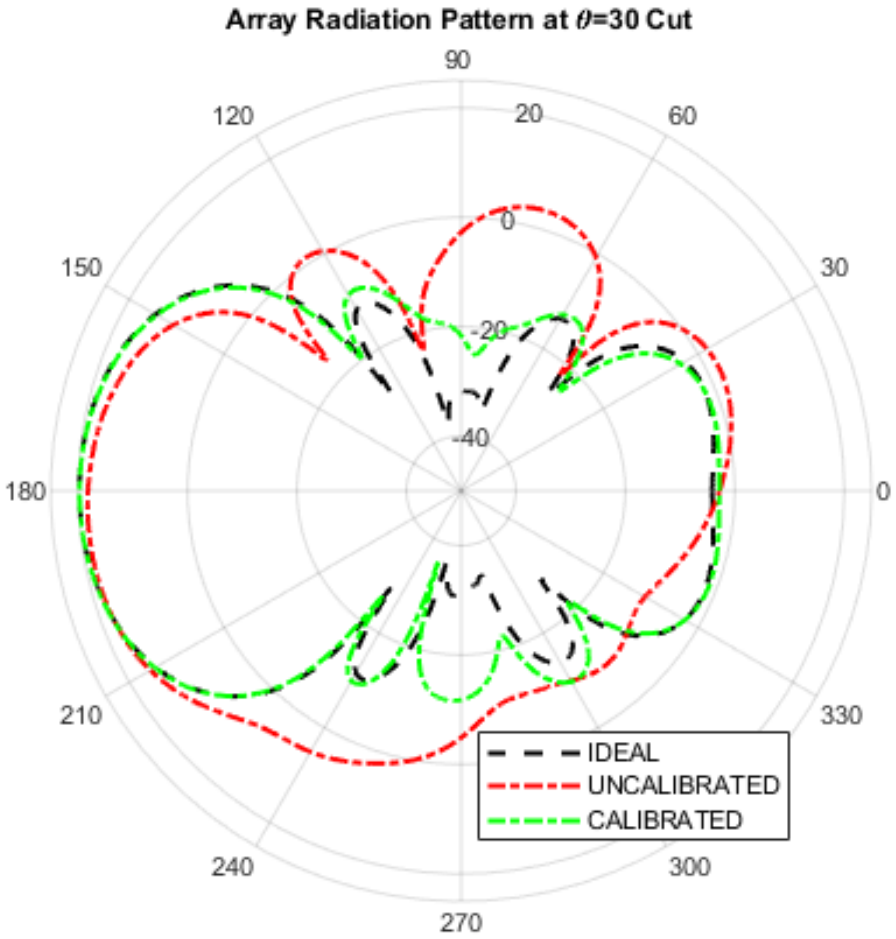

Figure 4.25. Radiation patterns for beam-steering angle $\theta_0 = 30^\circ$, $\phi_0 = 180^\circ$

Table 4.14. Numerical results for beam-steering angle $\theta_0 = 30^\circ$, $\phi_0 = 180^\circ$

	Main Lobe Direction (ϕ, θ)	*Gain*	*Beamwidth (3dB)*	*Side Lobe Level*
Ideal Case	180°	19.7 dBi	47.9°	-21.6 dB
Uncalibrated Case	188°	18.4 dBi	49.2°	-15.0 dB
Calibrated Case	180°	19.7 dBi	47.9°	-21.2 dB

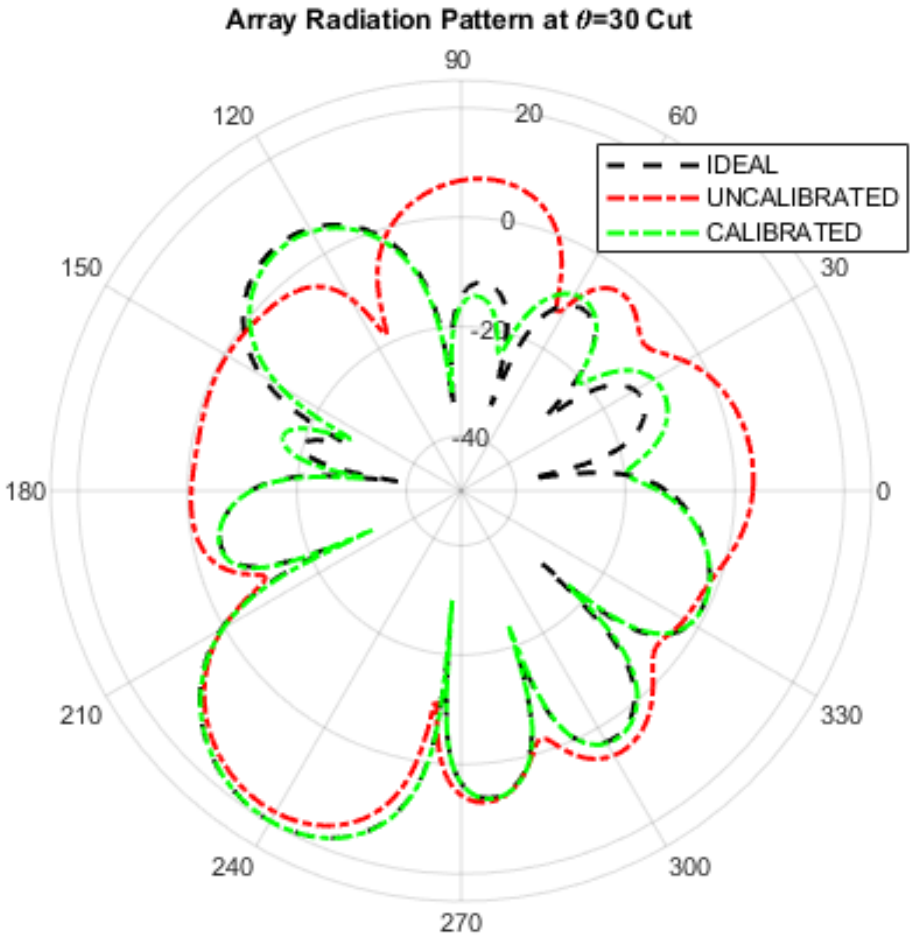

Figure 4.26. Radiation patterns for beam-steering angle $\theta_0 = 30^\circ$, $\phi_0 = 240^\circ$

Table 4.15. Numerical results for beam-steering angle $\theta_0 = 30^\circ$, $\phi_0 = 240^\circ$

	Main Lobe Direction (ϕ, θ)	*Gain*	*Beamwidth (3dB)*	*Side Lobe Level*
Ideal Case	240°	19.7 dBi	24.3°	-13.3 dB
Uncalibrated Case	238.8°	17.9 dBi	24°	-10.7 dB
Calibrated Case	240°	19.7 dBi	24.2°	-13.2 dB

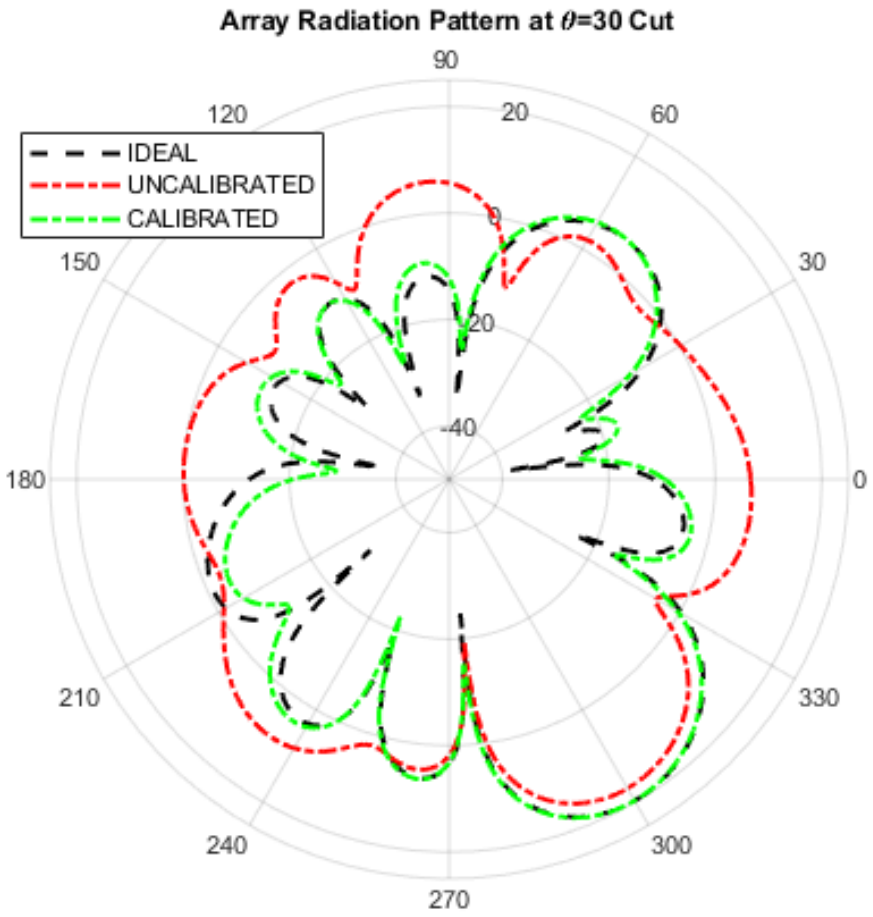

Figure 4.27. Radiation patterns for beam-steering angle $\theta_0 = 30^\circ$, $\phi_0 = 300^\circ$

Table 4.16. Numerical results for beam-steering angle $\theta_0 = 30^\circ$, $\phi_0 = 300^\circ$

	Main Lobe Direction (ϕ, θ)	*Gain*	*Beamwidth (3dB)*	*Side Lobe Level*
Ideal Case	300°	19.7 dBi	24.3°	-13.3 dB
Uncalibrated Case	300°	17.0 dBi	23.7°	-8.2 dB
Calibrated Case	300°	19.7 dBi	24.2°	-13.1 dB

The figures and tables above show that the parameters disrupted by error are compensated with the calibration process. Gains are improved by ~2 dBs, and the side lobe levels are improved by up to 5 dBs. In Figure 4.28, colormaps are used for further visual inspection of farfields in the orthographic uv projection plane.

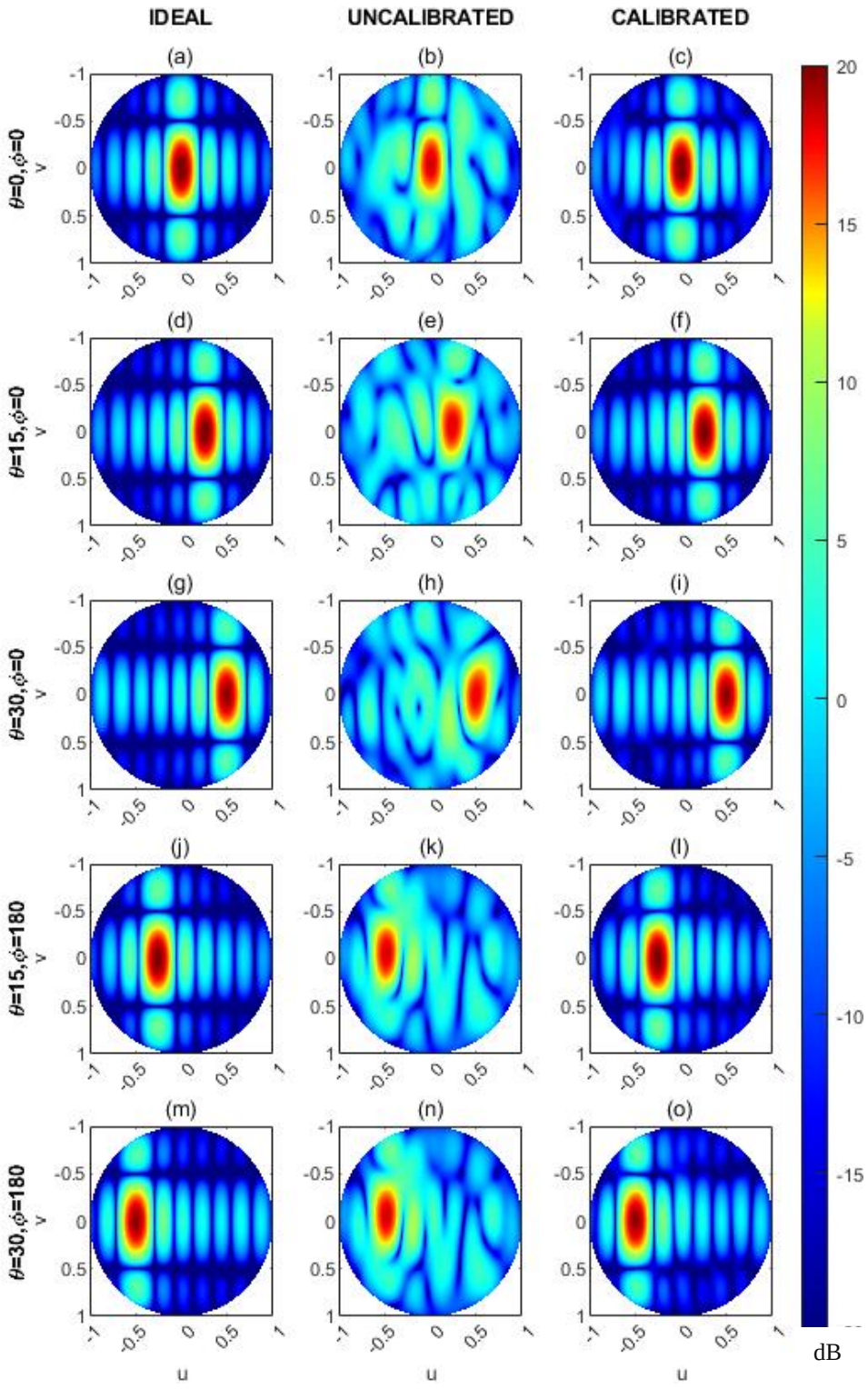

Figure 4.28. Orthographic projections of radiation patterns in uv-plane for ideal (a,d,g,j,m), uncalibrated (b,e,h,k,n) and calibrated (c,f,I,l,o) cases for different angles

For the different error distributions, first zero-mean distribution is simulated. As non-zero mean progressive phase shift error, 20° of mean error is added. As can be seen in uv-plots in Figure 4.29, this biased error resulted in completely different main lobe direction. However, thanks to calibration routine, the calibrated pattern is very close to the ideal pattern. This concludes that even with the presence of biased errors, the proposed algorithm can be applicable for the phased array antennas. Note that, uncalibrated pattern at $\theta = 30$ cut is not included in Figure 4.30 because uncalibrated case did not show meaningful pattern at $\theta = 30$ cut.

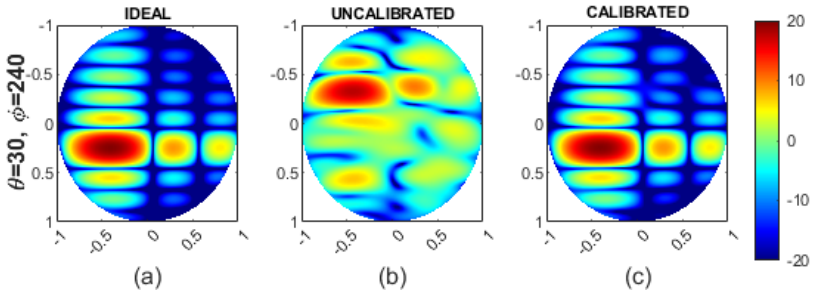

Figure 4.29. uv projections of radiation patterns with beam steering angle of $\theta_0 = 30^{\circ}$, $\phi_0 = 240^{\circ}$ with the presence of zero-mean error distributions for ideal (a), uncalibrated (b) and calibrated (c) cases

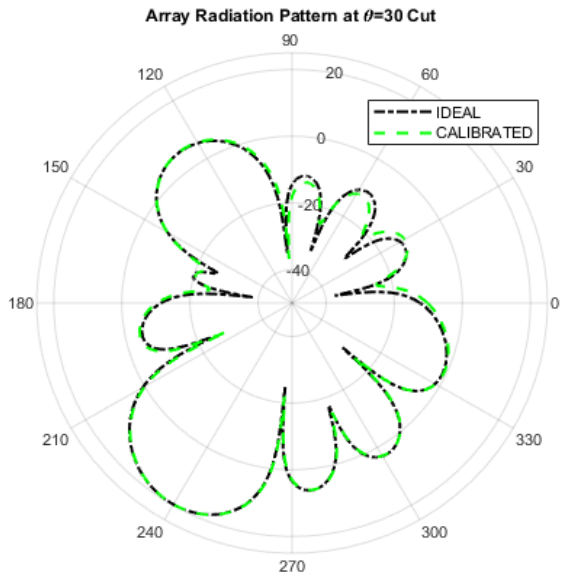

Figure 4.30. Radiation patterns for ideal and calibrated cases when 20° mean progressive phase error is present

For the dramatic case, 180° peak phase error is implemented. As seen from the Figure 4.31, the uncalibrated pattern shows completely random lobes and does not comply with the original pattern. After the calibration routine, the radiation pattern is appropriately aligned with the ideal case (Figure 4.32).

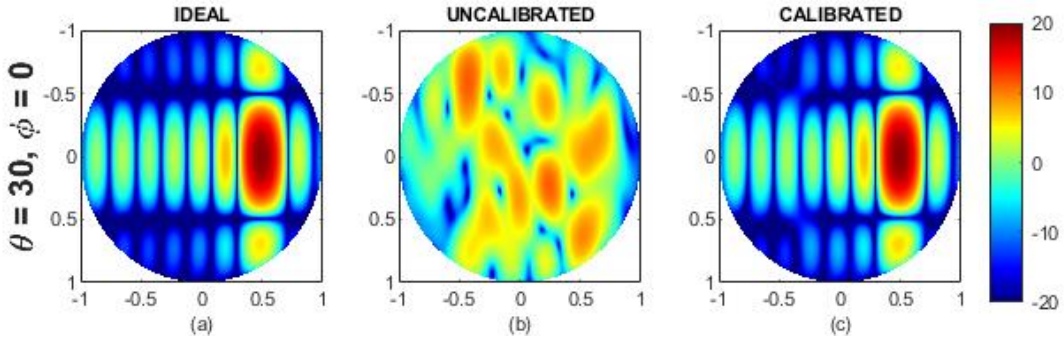

Figure 4.31. uv projections of radiation patterns with beam steering angle of $\theta_0 = 30^{\circ}$, $\phi_0 = 0^{\circ}$ with the presence of 180° peak phase error for ideal (a), uncalibrated (b) and calibrated (c) cases

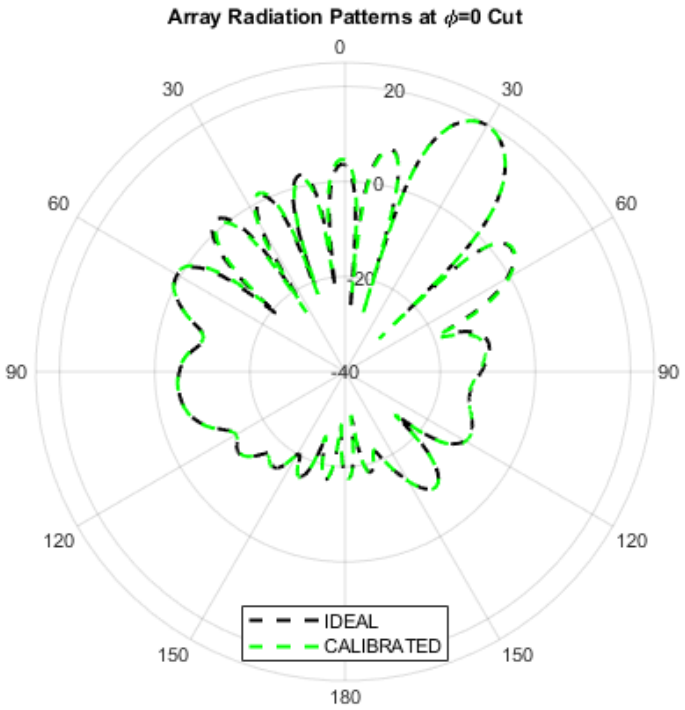

Figure 4.32. Radiation patterns for ideal and calibrated cases when 180° peak phase error is present

In the following, the amplitude tapered array is presented. In the simulations, Taylor distribution with four constant side lobes is implemented for the amplitudes to decrease SLLs.

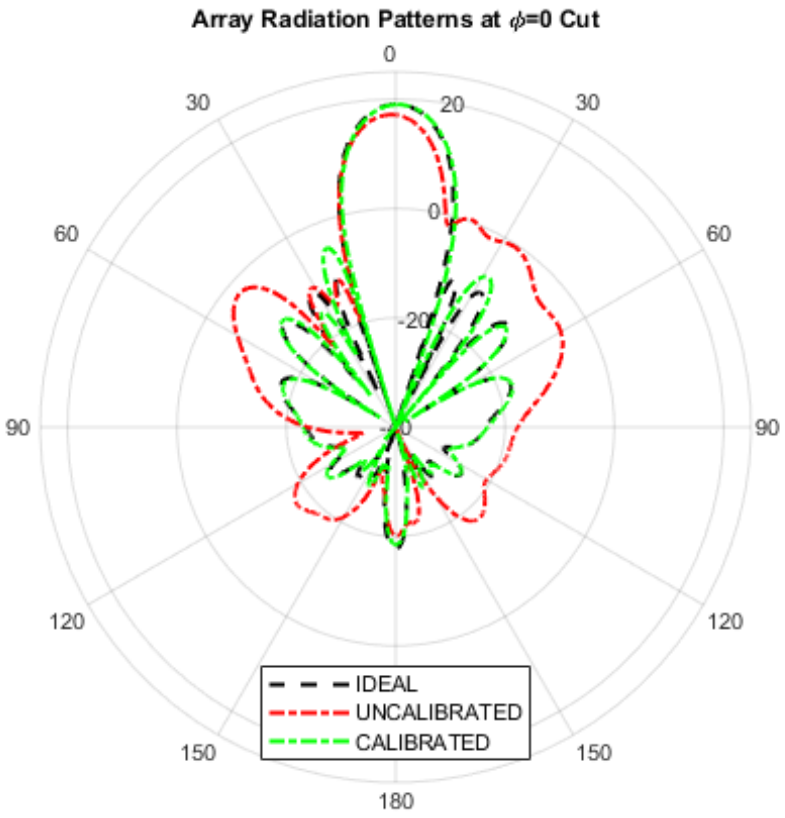

Figure 4.33. Radiation patterns for beam-steering angle $\theta_0 = 0^\circ$, $\phi_0 = 0^\circ$ with the presence of Taylor amplitude tapering

Table 4.17. Numerical results for beam-steering angle $\theta_0 = 0^\circ$, $\phi_0 = 0^\circ$ with the presence of Taylor amplitude tapering

	Main Lobe Direction (ϕ, θ)	*Gain*	*Beamwidth (3dB)*	*Side Lobe Level*
Ideal Case	0°	19 dBi	13.4°	-29.8 dB
Uncalibrated Case	1°	17.2 dBi	12.9°	-16.7 dB
Calibrated Case	0°	19 dBi	13.4°	-24.0 dB

4.3 Further Discussions on the Proposed Method

4.3.1 Robustness of the Proposed Method

Since the proposed method relies on erroneous phase responses of the phase shifters, there is a certain possibility that the correct phases may never present in the remapped phase responses. For example, if a phase shifter is required to alter the phase by $+11^{\circ}$ and the same phase shifter has no states that correlate with the requirement, the calibrated performance will be handicapped. In order to ensure the robustness of the calibration method, a Monte Carlo simulation sequence is performed with a constant steering angle which was $\theta_0 = 30^{\circ}$, $\phi_0 = 0^{\circ}$. At each simulation, ideal excitations are kept constant, but the random RMS error at each phase shifter and calibration routine is performed independently. As can be seen in Figure 4.34, the calibration results more or less stayed applicable.

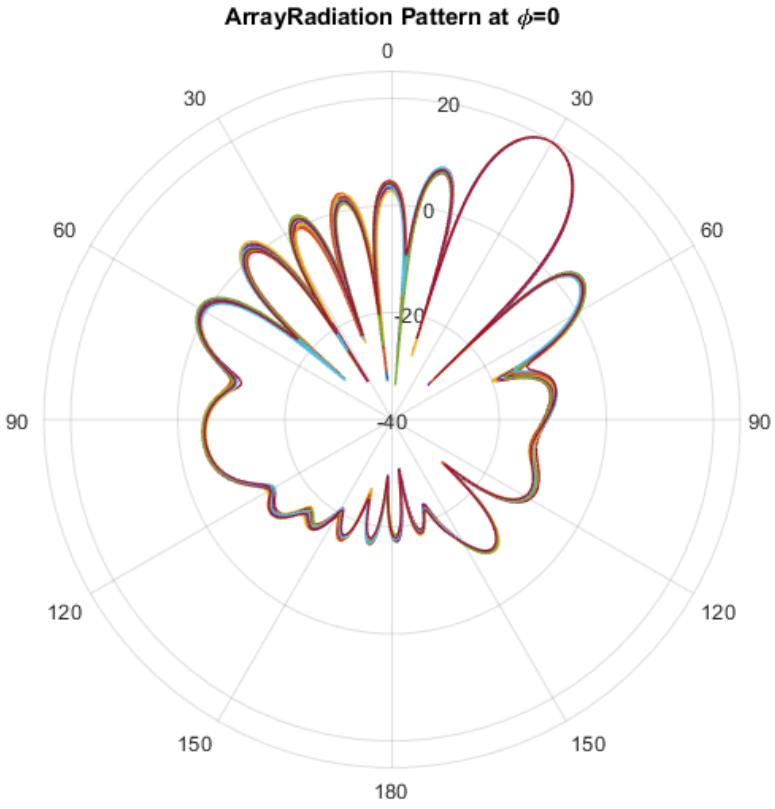

Figure 4.34. Calibration results for 20 different trials

4.3.2 Scalability of the Proposed Method

Given that the proposed method is validated for an 8 × 4 array, the scalability for large arrays can also be concluded. For validation, the 8 × 4 array was divided into two 4 × 4 sub-arrays meaning that the method is already scaled from 4 × 4 to 8 × 4 array. For larger arrays, using 4 × 4 blocks will be sufficient. The only challenge for a large array would be the first factory calibration. Since the proposed method requires prior antenna calibration, the first characterization of the antenna cells may become very time-consuming. An example scaled 16 × 16 array divided into 4 × 4 sub-arrays for calibration is given in Figure 4.35 and the simulated result for ideal, uncalibrated, and calibrated cases are given in Figure 4.36. All things considered; the method is scalable to large arrays with many cells.

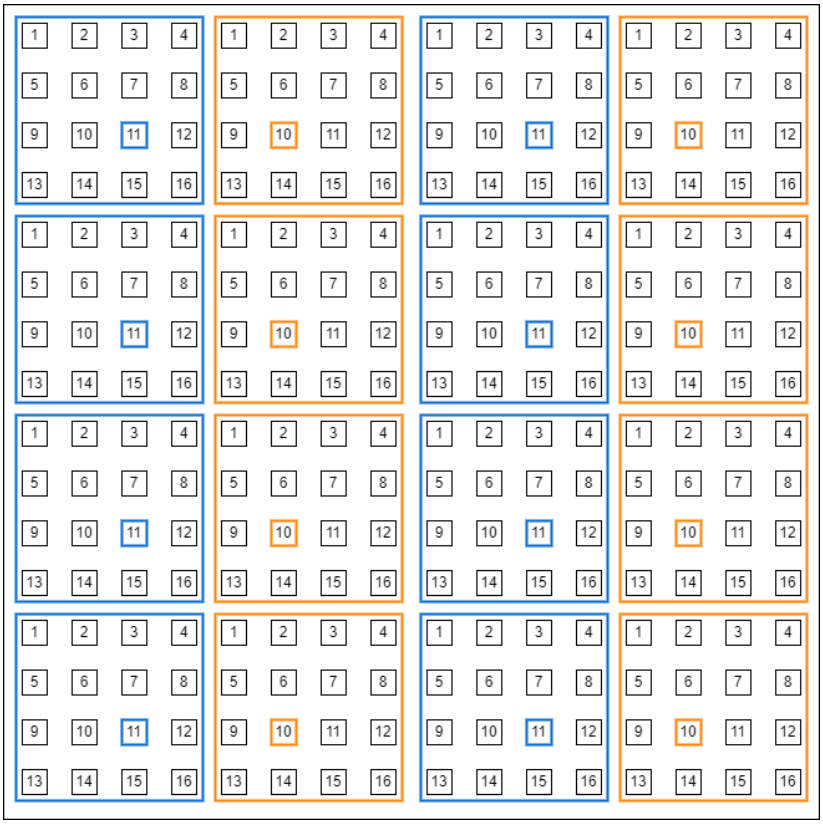

Figure 4.35. A 16 × 16 array antenna with 4 × 4 calibration sub-arrays

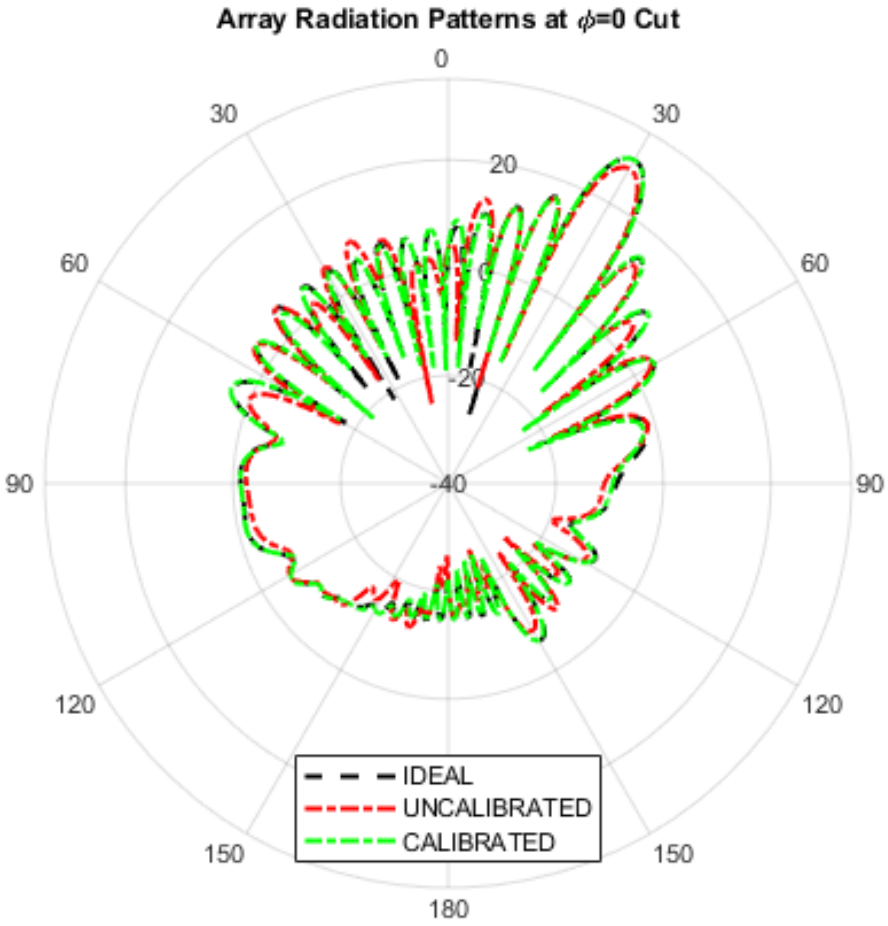

Figure 4.36. Simulated results for 16×16 array

4.3.3 Optimizing the Reference Antenna Count

As the size of the array increases, the count of the reference antennas may increase as well. However, if SNR levels for reference signals is high enough that the receiving antenna cell can register the signal, the count of the reference antenna can be reduced. To optimize the total count of the reference antennas, different square arrays are constructed with increasing dimensions. Note that, these arrays can be used as calibration sub-arrays for larger arrays. For each sub-array, the antenna cell in the middle is chosen as reference antenna and the average couplings are calculated.

Figure 4.37 shows the average couplings of each reference antenna for the increasing dimensions of the sub-arrays.

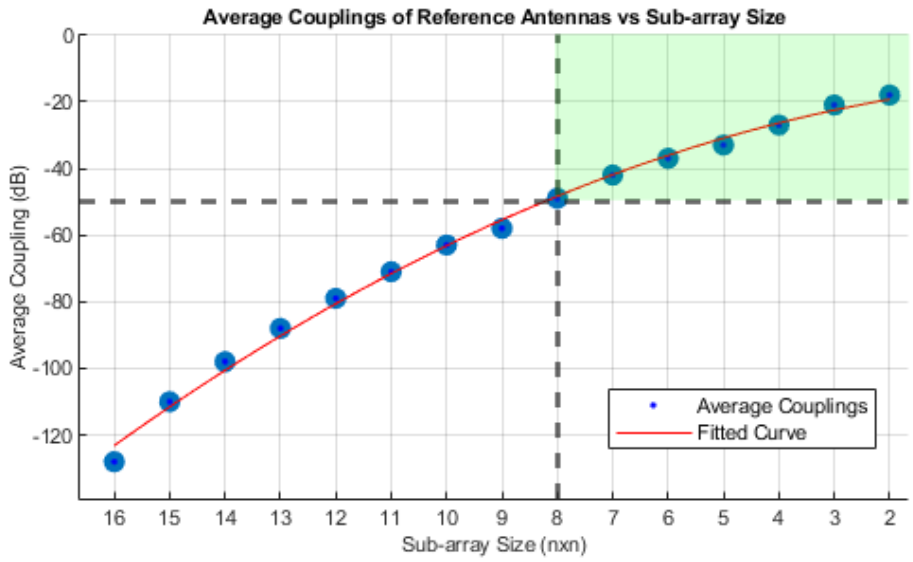

Figure 4.37. Average couplings of the reference antennas with applicable max sub array size (green area)

As the Figure 4.37 shows, above 8×8 sub-array size, the average couplings fall below -55 dB level, which is chosen as threshold for the applicable SNR levels for the calibration given the fact that most receivers have sensitivity of -60 dBm power levels with given bandwidth of the receiver (not considering pulse compression or other DSP Techniques). This scene can be improved by implementing lower NF of the receiver or higher output power for the reference signals. Nevertheless, saturation of the LNAs of adjacent elements should be avoided.

All things considered with the conditions mentioned above, 8×8 sub-array size would be the maximum sub-array size which minimizes the count of the total reference cells.

CHAPTER 5

CONCLUSION

This study presents the development of a spatially economic and self-aligning calibration method for airborne receive-only phased array antennas. A thorough literature survey has been carried out to identify the problem in detail. The survey found that most missile systems deploy semi-active seekers with phased array antennas. Later, the properties of phased array antennas are investigated. It is concluded that specific error sources for the phased array antenna cause performance degradation and undesired behavior. These errors are categorized according to their sources. Random error sources stem from the nature of the devices, and they are neither predictable nor calibrated; therefore, they are treated statistically. Drift errors in semiconductors appear because of the change in operating conditions and the semiconductor properties of the devices. They can be characterized and compensated via proper calibration. Finally, systematic errors of phased array antennas are investigated, and it is concluded that these errors can easily be eliminated through proper calibration routines. Considering all error sources combined, the final product's performance will differ from the desired numbers. Therefore, the necessity of calibration is legitimized.

Scrutinizing calibration methods, it is concluded that the best calibration method for the antenna depends on the application. For example, if there is a requirement for self-calibration capability, the mutual coupling and the peripheral fixed probes methods stand out. The mutual coupling is the best fit if the platform cannot tolerate any additional geometry for the antenna and calibration hardware. However, all calibration methods have their drawbacks. Even though the mutual coupling method stands out as the most applicable for the applications, it requires individual T/R modules for operation. In this thesis, the problem is defined for receive-only airborne antenna arrays. Therefore, the requirements include self-calibration capability with

no additional geometry and T/R modules. Having acquired the requirements, a hybrid method which is simply a combination of the mutual coupling method and the peripheral fixed probes method, is developed. Thanks to this method, instead of peripheral fixed probes, proper antenna cells are selected as the reference, and the characterization of the entire array is achieved through the coupling between antenna cells.

In the analysis section, for simulations, an 8×4 phased array antenna centered at 10 GHz with 200 MHz bandwidth is designed via CST and MATLAB-CST-API. After validation of the design, the beam-steering performance is confirmed for different theta and phi angles. After validation, the assignment of the reference antennas is carried out. For this purpose, the whole array simulation is conducted, and coupling ratios of each antenna cell are obtained. The average coupling ratios for each antenna cell are investigated to find the most suitable reference. The reference antennas are assigned with respect to the highest average coupling ratio to the cells in order to maximize calibration SNR. Later, the error modeling of the phased array antenna is implemented. The errors caused by deviations in phase shifters are reflected as RMS sum errors in the final phase response. During simulations, each phase shifter is affected by this additional error. Also, in order to simulate quantization errors, the real-world data from the datasheet of the modeled phase shifter is used. After creating an erroneous phase distribution, the calibration routine is implemented. In the proposed method, the algorithm remaps phase shifter states and 'defines' new phase shifters. Using these, the desired phase distribution is shown to be achievable. Later, to be fully convinced about the calibration method, the radiation patterns are compared between ideal, erroneous, and calibrated antennas. It is shown that the proposed method almost perfectly eliminates the errors, concluding that the antenna's performance is ensured for future missions.

After validating the proposed method, its robustness and scalability for larger arrays are discussed. Firstly, for robustness, since the method uses random fluctuation on the phase shifters, it is possible that the desired phases may never exist. In order to test the calibration method in terms of robustness, a Monte Carlo simulation with 20

trials is performed. In this simulation environment, the random errors and calibration routines are performed independently to simulate distinct antenna measurements. The results show that the calibration routine performed reasonably well in gain correction, side lobe level reduction, and beam pointing angle correction. From this result, it is concluded that the proposed method will perform as desired for the future missions of the platform. Secondly, the scalability property is discussed, and since the proposed method already uses sub-arrays to perform the task, the method is already scaled from a 4×4 to 8×4 antenna array. With this process, it is concluded that the proposed method can be scalable to arbitrarily large arrays, given that the reference antennas are assigned correctly.

In summary, a calibration method for airborne receive-only phased array antennas is developed and analyzed. Having defined and conducted a detailed literature search and come up with a proper solution, this study was a valuable experience for RF systems engineering. In future work, the next step will be implementing this calibration method on an existing antenna and validating the method in the experimental stage. For this purpose, a control circuitry and beamforming hardware should be implemented.

REFERENCES

[1] H. Hommel and H. P. Feldle, “Current status of airborne active phased array (AESA) radar systems and future trends,” in *IEEE MTT-S International Microwave Symposium Digest*, 2005, vol. 2005, pp. 1449–1452. doi: 10.1109/MWSYM.2005.1516962.

[2] J. A. Mittereder, J. A. Roussos, K. A. Christianson, and W. T. Anderson, “Reliability Life-Testing and Failure-Analysis of GaAs Monolithic Ku-Band Driver Amplifiers,” *IEEE Trans Reliab*, vol. 47, no. 2, pp. 119–125, 1998, doi: 10.1109/24.722272.

[3] A. Mehdi Bouchour, “Impact of aging on the behaviour of wild band gap power transistors, application to the efficiency of DC-DC converters,” Normandie Universite, 2020. [Online]. Available: https://tel.archives-ouvertes.fr/tel-03137632

[4] M. N. Al-M Oufti, S. v. Jaskolski, and T. Koryu Ishii, “Aging Effects on Bulk GaAs Devices,” *Proceedings of the IEEE*, vol. 56, no. 2, pp. 236–237, 1968, doi: 10.1109/PROC.1968.6255.

[5] H. Singh, H. L. Sneha, and R. M. Jha, “Mutual coupling in phased arrays: A review,” *International Journal of Antennas and Propagation*, vol. 2013. 2013. doi: 10.1155/2013/348123.

[6] A. A. Kishk, “Effect of the Misalignment of Antenna Elements in Phased Arrays,” *TENCON 2006 - 2006 IEEE Region 10 Conference*, pp. 1–3, 2006, doi: 10.1109/TENCON.2006.343722.

[7] I. Şeker, “Calibration methods for phased array radars,” in *Radar Sensor Technology XVII*, May 2013, vol. 8714, p. 87140W. doi: 10.1117/12.2015694.

[8] G. W. Stimson, *Introduction to airborne radar*. SciTech Pub, 1998.

[9] C. J. Baker and A. Zyweck, “Radar Missile Seekers,” in *Encyclopedia of Aerospace Engineering*, John Wiley & Sons, Ltd, 2010. doi: 10.1002/9780470686652.eae280.

[10] Naval Training Support Command, “Gunner’s Mate Missile M 3 & 2,” DC: US NAVY, 1972, p. 85.

[11] D. S. Bagri, “Pros and Cons of Using Arrays of Small Antennas versus Large Single-Dish Antennas for the Deep Space Network,” in *2009 IEEE Aerospace conference*, 2009, pp. 1–9. doi: 10.1109/AERO.2009.4839366.

[12] C. A. Balanis, *Antenna Theory: Analysis and Design*, 3rd ed. WILEY, 2012.

[13] Chetvorno, “Phased Array - Wikipedia,” Dec. 2016. https://en.wikipedia.org/wiki/Phased_array (accessed Jul. 02, 2022).

[14] P. D. Grant, R. R. Mansour, and M. W. Denhoff, “A Comparison Between RF MEMS Switches and Semiconductor Switches,” in *2004 International Conference on MEMS, NANO and Smart Systems (ICMENS’04)*, 2004, pp. 515–521. doi: 10.1109/ICMENS.2004.1509004.

[15] A. Combs, “Application Note AN-007: A Comparative Review of GaN, LDMOS, and GaAs for RF and Microwave Applications,” 2008. https://nuwaves.com/wp-content/uploads/2020/08/AN-007-A-Comparative-Review-of-GaN-LDMOS-and-GaAs-for-RF-and-Microwave-Applications.pdf (accessed Jul. 25, 2022).

[16] S. Rathod, K. Sreenivasulu, K. S. Beenamole, and K. P. Ray, “Evolutionary trends in transmit/receive module for active phased array radars,” *Def Sci J*, vol. 68, no. 6, pp. 553–559, Nov. 2018, doi: 10.14429/dsj.68.12628.

[17] “TGP2105-SM 6-18 GHz 6-Bit Digital Phase Shifter (+Vc),” 2017. https://www.qorvo.com/products/p/TGP2105-SM (accessed Jul. 25, 2022).

[18] G. v Tsoulos and M. A. Beach, “Calibration and Linearity issues for an Adaptive Antenna System,” in *1997 IEEE 47th Vehicular Technology*

Conference. Technology in Motion, 1997, pp. 1597–1600. doi: 10.1109/VETEC.1997.605827.

[19] A. Vasic, M. Vujisic, B. L. Jovanovic, K. Stankovic, and B. Jovanovic, "Ambiguous Influence of Radiation Effects in Solar Cells," in *Progress in Electromagnetics Research Symposium*, 2010, pp. 1990–1203.

[20] R. H. Maurer, K. Chao, C. Brent Bargeron, and R. C. Benson, "Reliability of gallium arsenide devices," *Johns Hopkins APL Tech Dig*, vol. 13, no. 3, pp. 407–417, 1992.

[21] S. Kayali, G. Ponchak, and R. Shaw, "GaAs MMIC Reliability Assurance Guideline forSpace Applications," *Jet Propultion Laboratory*. NASA, Tech Rep., 1996.

[22] G. He, X. Gao, and R. Zhang, "Impact Analysis and Calibration Methods of Excitation Errors for Phased Array Antennas," *IEEE Access*, vol. 9, pp. 59010–59026, 2021, doi: 10.1109/ACCESS.2021.3073222.

[23] H. M. Aumann, A. J. Fenn, and F. G. Willwerth, "Phased Array Antenna Calibration and Pattern Prediction Using Mutual Coupling Measurements," *IEEE Trans Antennas Propag*, vol. 37, no. 7, pp. 844–850, 1989, doi: 10.1109/8.29378.

[24] D. A. James, *Radar Homing Guidance for Tactical Missiles*, 1st ed. 1986. doi: 10.1007/978-1-349-08602-3.

[25] Z. Iqbal and M. Pour, "Grating Lobe Reduction in Scanning Phased Array Antennas with Large Element Spacing," *IEEE Trans Antennas Propag*, vol. 66, no. 12, pp. 6965–6974, Dec. 2018, doi: 10.1109/TAP.2018.2874717.

[26] S. 'Symeonidis and S. 'Mitilineos, "MATLAB CST API." 2018. doi: 10.5281/zenodo.1237969.